

IMPACT AND INTERPLAY OF Λ CDM ANALYSIS CHOICES FOR LSST COSMIC SHEAR

N. C. ROBERTSON^{1*}, C. HEYMANS^{1,2}, J. ZUNTZ¹, P. BURGER^{3,4}, C. D. LEONARD⁵, I. G. MCCARTHY⁶, J. C. PAINE⁷,
 J. SALCIDO⁶, N. ŠARČEVIĆ⁸, M. SCHALLER^{9,10}, J. SCHAYE¹⁰, M. P. VAN DAALEN¹⁰ THE FLAMINGO TEAM AND
 THE LSST DARK ENERGY SCIENCE COLLABORATION.
Author affiliations may be found before the references.

Version February 26, 2026

ABSTRACT

We forecast cosmological parameter constraints for a cosmic shear analysis of the Rubin Observatory Legacy Survey of Space and Time (LSST), defining an analysis framework that can accurately recover the Λ CDM model in the presence of astrophysical and data-related systematics. When accounting for our present uncertainty on the suppression of the non-linear matter power spectrum through baryon feedback, we find that the error on the composite parameter $S_8 = \sigma_8 \sqrt{\Omega_m/0.3}$ almost doubles compared to an LSST analysis which neglects this astrophysical phenomenon. After the first year of observations, LSST will extend beyond the magnitude limit of existing representative spectroscopic calibration samples, requiring photometric redshifts to be calibrated using an alternative strategy. Adopting literature measurements of the reduced redshift calibration precision found from galaxy cross-correlation techniques, combined with current levels of baryon feedback uncertainty, we forecast final year LSST cosmic shear constraints that barely improve upon the first year analysis. This forecast therefore serves as encouragement to the community to develop methodology and observations to constrain models of baryon feedback and enhance photometric redshift calibration at depths where spectroscopy is unrepresentative. With tight priors on both these systematic terms, we forecast that LSST cosmic shear can deliver constraints on S_8 that are more than five times as constraining as existing cosmic shear surveys.

Keywords: methods: statistical – dark energy – large-scale structure of the universe

CONTENTS

| | |
|--|----|
| 1. Introduction | 1 |
| 2. Methodology | 3 |
| 2.1. Data-related systematics | 3 |
| 2.2. Baryon Feedback | 4 |
| 2.2.1. Building mock data using FLAMINGO | 4 |
| 2.2.2. Scale Cuts | 5 |
| 2.2.3. Fiducial analysis with HMCODE2020 | 5 |
| 2.2.4. Alternative analysis with SP(K) | 7 |
| 2.3. Intrinsic Galaxy Alignment | 7 |
| 2.4. Posterior Summary Statistics and Projection Effects | 7 |
| 3. Results | 8 |
| 3.1. Defining the fiducial Y1 analysis | 8 |
| 3.2. Varying the baryon feedback strength and model | 9 |
| 3.3. Varying survey depth: analysing Y10 | 11 |
| 3.4. Varying the intrinsic alignment model | 12 |
| 3.5. Joint Constraints in $w_0 - w_a$ CDM | 12 |
| 4. Conclusions | 13 |
| A. Cosmic Shear Theory | 16 |
| B. Mock LSST Observations | 17 |
| C. Cosmological Parameters and Priors | 18 |
| C.1. Sensitivity to the parameter set: σ_8 or A_s | 18 |
| C.2. Sensitivity to the informative prior width: h_0 and n_s | 18 |
| C.3. Varying the sum of neutrino masses | 19 |
| D. Sampler Choice | 19 |
| E. Mitigating projection bias | 20 |
| F. Additional Data Tables and Figures | 21 |
| F.1. Modelling intrinsic alignments with TATT | 21 |
| F.2. Data tables | 21 |

1. INTRODUCTION

Cosmology has entered a new era with the Vera C. Rubin Observatory and *Euclid* satellite now building deep ‘full-sky’ surveys¹, exceeding the statistical power of all precursor imaging surveys. The study of weak gravitational lensing by large-scale structure, known as ‘cosmic shear’, is a primary science driver for both *Euclid* and *Rubin* and the focus of this study. Cosmic shear measures the observed lensing-induced correlation between galaxy shapes as a function of redshift, mapping both the growth of large-scale structures and the expansion history of the Universe (see [Huterer 2023](#), and references therein).

The most recent precursor lensing surveys are close to completion: Dark Energy Survey (DES, [Bechtol et al. 2025](#)), Dark Energy Camera All Data Everywhere (DECADE, [Anbajagane et al. 2025](#)), Hyper Suprime-Cam (HSC, [Aihara et al. 2022](#)), Kilo-Degree Survey (KiDS, [Wright et al. 2024](#)). The primary weak lensing constraints made by these surveys are on the parameter $S_8 \equiv \sigma_8 \sqrt{\Omega_m/0.3}$, which combines the matter density parameter, Ω_m , and the density fluctuation amplitude parameter σ_8 . While these surveys find consistent percent-level measurements of these parameters (see [DES Collaboration et al. 2026](#); [Wright et al. 2025b](#); [Dark Energy Survey and Kilo-Degree Survey Collaboration et al. 2023](#), hereafter DK23, and references therein), there has been a degree of tension between them and equivalent CMB-derived measurements (see for example [Di Valentino et al. 2021](#)). Efforts to understand differences have shone a spotlight on the various sources of astrophysical and data-related systematics in weak lensing studies ([Mandelbaum 2018](#)). By taking a conservative approach to modelling these uncertainties,

¹ The *Euclid* Wide Survey will image the ‘full’ extragalactic sky outside the galactic and ecliptic planes, spanning roughly 14,000 square degrees ([Euclid Collaboration et al. 2025b](#)). The *Rubin* Legacy Survey of Space and Time (LSST) will image the ‘full’ Southern sky, spanning between 15,000 and 18,000 square degrees ([Lochner et al. 2022](#)).

* Email: naomi.robertson@ed.ac.uk

the precursor cosmic shear surveys are already limited from realising their full statistical power (DK23), a potentially problematic situation for *Euclid* and *Rubin*.

A key missing ingredient from early *Euclid* and *Rubin* forecasts in Laureijs et al. (2011) and The LSST Dark Energy Science Collaboration: Mandelbaum et al. (2018, hereafter DESC-SRD²), was the significant uncertainty in the theoretical modelling of the total matter distribution on small physical scales ($k > 0.1h\text{Mpc}^{-1}$). Using gravity-only N -body simulations, the non-linear matter distribution can be accurately determined either directly via an emulator (Heitmann et al. 2014; Euclid Collaboration: Knabenhans et al. 2021; DeRose et al. 2023; Chen et al. 2025), or indirectly using a simulation-calibrated halo model (Takahashi et al. 2012; Mead et al. 2015). What these studies neglect, however, is the power that non-gravitational forces, particularly Active Galactic Nuclei (AGN), have to locally re-distribute both baryonic and dark matter (White 2004; Semboloni et al. 2011; van Daalen et al. 2011). Known as ‘baryon feedback’, the significance of this astrophysical effect can be estimated using hydrodynamical simulations (Schaye et al. 2010; van Daalen et al. 2020; Schaye et al. 2023; Salcido et al. 2023; Pakmor et al. 2023; McCarthy et al. 2023; Martin-Alvarez et al. 2025), analytical halo models (Debackere et al. 2020; Mead et al. 2021), or a process called ‘baryonification’ whereby halo profiles in gravity-only simulations are modified to replicate different feedback scenarios (Schneider & Teysier 2015; Aricò et al. 2021; Anbajagane et al. 2024).

Updated forecasts for *Euclid* and *Rubin* have assessed the impact of baryon feedback, quantifying the challenges related to this astrophysical systematic in a scenario where all other data-quality requirements are met. Martinelli et al. (2021) conclude that even for a ‘pessimistic’ *Euclid* analysis that removes projected small-scale cosmic shear information ($\ell_{\text{max}} = 1500$), halving the nominal *Euclid* dark energy figure of merit, the bias introduced from unmodelled baryon feedback is potentially significant enough to lead to a false detection of a time-varying dark energy equation of state. Semboloni et al. (2013); Huang et al. (2019); Spurio Mancini & Bose (2023); Boruah et al. (2024) demonstrate how removing small scale cosmic shear data and marginalising over a set of nuisance parameters to model the baryon feedback can remove this bias to the recovered cosmological parameters, at the cost of a loss in precision. Huang et al. (2019) find that baryon feedback modelling roughly doubles the *Rubin* errors on the dark energy parameters. All studies concluded that the original forecast choice to mitigate baryon feedback through scale cuts alone, with $\ell_{\text{max}} = 3000$ for *Rubin* or $\ell_{\text{max}} = 5000$ for *Euclid*, was not a viable approach.

Recent results from the BAHAMAS, ANTILLES, FLAMINGO and XFABLE suites of hydrodynamical simulations (McCarthy et al. 2017; Salcido et al. 2023; Schaye et al. 2023; Bigwood et al. 2025b) serve to complicate the situation further. These simulations are the first to reproduce the observed hot gas fraction in groups and clusters, the galaxy stellar mass function and the distribution of galaxy sizes in large cosmological volumes. They predict that baryon feedback could suppress the clustering of matter on physical scales as large as $\sim 60\text{Mpc}$ ($k \sim 0.15h\text{Mpc}^{-1}$), which is also predicted by halo models constrained by observed cluster gas fractions (Debackere et al. 2020). In comparison, existing forecasts have primarily considered scenarios where baryon feedback only becomes significant on scales $k \gtrsim 1h\text{Mpc}^{-1}$. Observational evidence supports these

more extreme models in the form of cross-correlation studies of weak lensing with either measurements of the thermal Sunyaev-Zel’dovich (SZ) effect (Amodeo et al. 2021; Tröster et al. 2022; Pandey et al. 2023; McCarthy et al. 2023; To et al. 2024; Dalal et al. 2025; La Posta et al. 2025), or the diffuse X-ray background (Ferreira et al. 2024), along with joint analyses of lensing with the kinetic-SZ effect (Bigwood et al. 2024; McCarthy et al. 2025; Hadzhiyska et al. 2025; Sunseri et al. 2025; Siegel et al. 2025b). Strong baryon feedback is also supported by studies of the thermal-SZ autopower spectrum (Reichardt et al. 2021; Bolliet et al. 2018) and fast radio bursts (Reischke & Hagstotz 2025). These results motivate re-establishing the cosmic shear analysis choices for the next generation of imaging surveys. We note that while we analyse a mock Legacy Survey of Space and Time (LSST) for the first year of *Rubin*, our findings can be broadly applied to the *Euclid* Wide Survey given the similarities in survey area and effective depth.

In this analysis we present cosmic shear forecasts for the first year (Y1) and final tenth year (Y10) of LSST, within a flat- Λ CDM cosmological model. Our main focus is the impact of baryonic effects, as described above, but we also consider the interplay of our fiducial baryon model with a set of other effects: the influence of samplers, priors and the chosen parameter space; the effect of adopting two different models to account for the intrinsic alignment of galaxies (see Chisari 2025, and references therein); and the possibility that Y10 will not reach its required photometric redshift accuracy. With current techniques and instrumentation, the uncertainty on the redshift distribution of the Y10 sample will degrade relative to the Y1 sample, owing to the lack of a representative deep spectroscopic survey. Such a sample exists for Y1 depths (Stanford et al. 2021), allowing for an accurate and precise calibration of redshift distributions via machine learning methods (see Newman & Gruen 2022, and references therein). The alternative calibration route for deep imaging surveys relies on clustering measurements between photometric and spectroscopic galaxy samples, where the spectroscopy spans the full redshift range, even if it is incomplete in colour-colour space (Newman 2008). Unfortunately this promising approach has only realised a redshift calibration precision that is more than an order of magnitude larger than the DESC-SRD Y10 requirement, limited by astrophysical uncertainty related to magnification and non-linear galaxy bias (Hildebrandt et al. 2021; Gatti et al. 2022; Wright et al. 2025a). We forecast how this level of degradation in the uncertainty on the redshift distribution will impact the Y10 constraints.

Our approach differs from many previous *Rubin* and *Euclid* studies primarily because they forecast the w_0w_a CDM model, constraining a time varying dark energy equation of state. Given that it has been argued that the hints of tension currently seen between independent probes for the Λ CDM model could be attributed to unmodelled systematic errors (Amon & Efstathiou 2022; Preston et al. 2023; Elbers et al. 2025), we seek to first define an analysis framework that can recover unbiased Λ CDM constraints from a realistic mock of LSST. We argue that only if tensions and systematics in this subspace are fully understood is it safe to combine cosmic shear with the other data sets needed to obtain our target percent level constraints on the w_0w_a CDM cosmological model. As such, we focus on a Λ CDM forecast and only include w_0w_a CDM forecasts in Section 3.5 as a means to compare our findings to other studies.

We have chosen to consider cosmic shear alone in this study, in contrast to creating a joint ‘ 3×2 pt’ forecast which combines cosmic shear with galaxy clustering and galaxy-galaxy lensing (Heymans et al. 2021; DES Collaboration

² DESC-SRD: the Dark Energy Science Collaboration - Science Requirements Document.

et al. 2026; Porredon et al. 2025). In the case where the set of adopted systematics models and priors provide an accurate representation of the underlying truth, a ‘3×2pt’ analysis will certainly help to self-calibrate the systematics that limit cosmic shear. In the more realistic scenario, however, where the models are only approximate, the combination of model bias alongside the known interplay between the different systematic parameters can lead to errors in the joint constraints (Fischbacher et al. 2023; Samuroff et al. 2024; Leonard et al. 2024). It is therefore important that each probe is explored and understood individually before moving forward with a joint analysis.

This paper is organised as follows: we introduce the cosmic shear analysis framework in Section 2, discussing both data-related and astrophysical systematic models along with our metric of success for the recovery of the input cosmological parameters. Section 3 presents our Λ CDM forecasts, determining the rationale for our fiducial analysis of LSST-Y1 and exploring the robustness of that analysis to variations in the baryon feedback strength, survey depth and the intrinsic alignment model. In this forecast we sample the full likelihood instead of taking the more traditional Fisher matrix approach (Wolz et al. 2012). For our w_0w_a CDM forecasts in Section 3.5, we explore weak lensing forecasts in combination with Gaussian priors based on the current generation of external data sets, minimising the computational expense of a full multi-probe forecast. We conclude in Section 4. The main body of the paper is supplemented by a series of appendices: Appendix A reviews the cosmic shear theory and the emulator used to rapidly calculate likelihoods; Appendix B discusses the creation of mock LSST cosmic shear observations; Appendix C motivates our choice of cosmological parameter space and priors; Appendix D considers three different sampling algorithms and discusses our reasons for adopting NAUTILUS³ (Lange 2023) for our analysis; Appendix E details our approach to mitigate projection bias in our analysis; Appendix F tabulates our key results along with additional figures of our constraints in extended parameter spaces.

2. METHODOLOGY

We create mock cosmic shear observables for LSST-Y1 and Y10 using a five-bin tomographic convergence power spectrum C_ℓ , implemented within COSMOSIS (see Zuntz et al. 2015, and Appendix A). Our ingredients are listed in Table 1, where we adopt the DESC-SRD parameters for LSST depth, area and expected data quality in terms of shear and redshift precision (for more detail see Appendix B).

In Table 2 we list the parameters of the ‘truth’ input cosmological model and astrophysical systematic models, compared to the set of priors that we adopt in our likelihood analysis. The rationale for our choice of input cosmological parameters and priors is presented in Appendix C. For reference, Table 2 also includes the DESC-SRD adopted priors which in most cases are more informative. In this section we discuss how we model data-related systematics, baryon feedback and intrinsic galaxy alignment.

2.1. Data-related systematics

Cosmic shear measures the lensing induced by the projected mass distribution along the line of sight. The signal is therefore highly sensitive to the mean redshift of the galaxy population. In this study, we limit our model of the redshift calibration uncertainty for each tomographic bin to a single parameter that measures the bias in the mean redshift, δ_z^i such that $n_{\text{estimate}}^i(z) = n_{\text{true}}^i(z + \delta_z^i)$. We take a different approach from DESC-SRD: instead of calculating the

required limit for δ_z^i to ensure LSST achieves a particular figure of merit, we ask what is feasible given current instrumentation and methodology.

At Y1 depth, the photometric galaxy sample is well-matched to the C3R2 spectroscopic survey, designed to provide galaxy spectroscopy for a sample that is complete in colour-space to $i \sim 24.5$ (10σ extended source, Stanford et al. 2021). With C3R2, Y1 photometric redshifts can be calibrated using self-organising maps (SOM) and a two-step process utilising the Deep Drilling Fields to improve the calibration accuracy for the Wide survey (see for example Buchs et al. 2019; Wright et al. 2020; McCullough et al. 2024; Yin et al. 2025). Stanford et al. (2021) demonstrate that the existing C3R2 sample can already deliver an accuracy of $\delta_z \sim 0.002(1+z)$ for 92% of the *Euclid* sample, which is slightly deeper than Y1. As C3R2 continues to collect data, we adopt $\delta_z^i \sim 0.002(1+z_i)$ for our fiducial Y1 forecast, which also matches the DESC-SRD requirement. We adopt a multivariate Gaussian prior⁴ for the vector of redshift nuisance parameters, δ_z^i , in order to implement an assumed 20% correlation in the redshift uncertainty between neighbouring bins and a 5% correlation between non-neighbouring bin pairs, as motivated by Hildebrandt et al. (2021); Cordero et al. (2022).

At Y10 depth, photometric redshift calibration will most likely be determined using cross-correlation techniques (Newman 2008). By measuring the angular clustering between the Y10 photometric sample and a luminous spectroscopic sample that spans the full redshift range, the redshift distribution of each tomographic bin can be estimated. For Stage-III surveys, the accuracy of this approach has been shown to be limited by uncertainty on the magnification and galaxy bias model for the spectroscopic sample. This results in a calibration uncertainty $\delta_z^i \sim 0.015$ that is broadly independent of redshift (Hildebrandt et al. 2021; Gatti et al. 2022; Newman & Gruen 2022). In principle, the spectroscopic galaxy bias could be self-calibrated using a ‘6 × 2pt’ analysis, cross-correlating the shear with itself and the photometric and spectroscopic samples, in addition to auto- and cross-clustering of the two galaxy samples (Bernstein 2009). As this approach remains under development, however (see the successes and challenges discussed in Johnston et al. 2025), we choose to adopt $\delta_z^i = 0.015$ for our Y10-like forecast, including an optimistic scenario variant with $\delta_z^i \sim 0.001(1+z_i)$.

In this analysis we limit our modelling of redshift uncertainty to the standard δ_z^i linear shift parameters, assuming that the outlier population is known accurately. This approach is sufficient for current surveys (Stölzner et al. 2021; Amon et al. 2022), but for LSST and *Euclid*, additional $n(z)$ nuisance parameters will be required to ensure the accurate recovery of cosmological constraints (Boruah et al. 2024; Mill et al. 2025; DES Collaboration et al. 2026). The community has yet to converge on an optimal approach to flexibly model the $n(z)$ (Stölzner et al. 2021; Cordero et al. 2022; Myles et al. 2023; Ruiz-Zapatero et al. 2023; Zhang et al. 2023b; Reischke 2024; Bernstein et al. 2025; d’Assignies et al. 2025).

For each tomographic bin i , we marginalise over our uncertainty on the calibration of the measured shear, σ_m^i , following Li et al. (2023), who simulate a range of different galaxy morphology distributions to quantify the shear calibration uncertainty arising from imperfect image simulations. Assuming that numerous image simulations can be analysed to minimise statistical noise on the shear calibra-

⁴ This can be implemented using the `correlated_priors` module within COSMOSIS which uses a Cholesky decomposition of the covariance matrix between nuisance parameters to create multivariate parameters that follow normal distributions.

³ NAUTILUS: nautilus-sampler.readthedocs.io/

| Mock Ingredient | Information | Reference |
|--|---|--|
| Linear matter power spectrum | CAMB | Lewis et al. (2000); Howlett et al. (2012) |
| Gravity-only non-linear power spectrum | HMCODE2020 with no feedback | Mead et al. (2021) |
| Baryon Feedback Suppression | FLAMINGO ‘L1_m9’ | Schaye et al. (2023) |
| Intrinsic Alignment model | Non-linear linear alignment (NLA-z) | Bridle & King (2007); Joachimi et al. (2011) |
| Cosmic Shear Statistic | Convergence Power Spectrum C_ℓ | Kilbinger et al. (2017), equation 43(ii) |
| Number of ℓ bins | 24 log-spaced | |
| Mock ℓ -range | $\ell = [20, 5000]$ | |
| Ellipticity Variance | $\sigma_e = 0.26$ | DESC-SRD: appendix D2.1 |
| Masked area fraction | $f_{\text{mask}} = 0.12$ | " appendix F1 |
| Number of Redshift Bins | 5, equal numbers in each bin | " appendix D2.1 |
| Photometric Redshift Error | $p(z_p z_{\text{true}}) = \mathcal{N}[\mu = z_{\text{true}}; \sigma = 0.05(1 + z_{\text{true}})]$ | " appendix D2.1 |
| Known Photometric Redshift Outliers | 7% uniformly distributed between $0 < z < 3$ | |
| Y1 Area | 12,300 deg ² | " appendix C1 |
| Y1 Depth (5σ point source) | $i < 24.13$ | " appendix C1 |
| Y1 Number density | $n_{\text{eff}} = 11.112 \times (1 - f_{\text{mask}}) = 9.78 \text{ arcmin}^{-2}$ | " table F1 |
| Y1 Redshift Distribution | $n(z) \propto z^2 \exp[-(z/0.13)^{0.78}]$ $\bar{z} = 0.85$ | " figure F4 |
| Y10 Area | 14,300 deg ² | " appendix C1 |
| Y10 Depth (5σ point source) | $i < 26.35$ | " appendix C1 |
| Y10 Number density | $n_{\text{eff}} = 27.737 \times (1 - f_{\text{mask}}) = 24.4 \text{ arcmin}^{-2}$ | " table F1 |
| Y10 Redshift Distribution | $n(z) \propto z^2 \exp[-(z/0.11)^{0.68}]$ $\bar{z} = 1.05$ | " figure F4 |

Table 1. A list of ingredients for mock cosmic shear observations of LSST-Y1 and Y10: the input theoretical models for the cosmological and contaminating signals; the cosmic shear statistic; the simulated data quality in terms of shear and redshift precision; Y1 and Y10 survey parameters. References are provided in the final column and discussed in Appendices A and B. We note that the LSST survey footprint will remain under review throughout the survey’s lifetime, with the final area expected to be closer to 18,000 deg², $\sim 25\%$ larger than the DESC-SRD survey parameters adopted in this analysis. As we find that our LSST cosmic shear forecasts are systematics dominated, an increase in survey area would not impact our conclusions.

| | Input | DESC-SRD | Fiducial Analysis | Informed? |
|--|--------------------------|---|---|-----------|
| Cosmological parameter priors: | | | | |
| Amplitude | $\sigma_8 = 0.8$ | $\sigma_8 : \mathcal{N}(0.831; 0.14)$ | $\sigma_8 : [0.39; 1.01]$ | ✗ |
| Hubble constant | $h = 0.715$ | $h : \mathcal{N}(0.6727; 0.063)$ | $h : [0.65; 0.78]$ | ✓ |
| Matter density | $\Omega_m = 0.3$ | $\Omega_m : \mathcal{N}(0.3156; 0.2)$ | $\Omega_m : [0.2; 0.46]$ | ✗ |
| Baryon density | $\omega_b = 0.02233$ | $\Omega_b : \mathcal{N}(0.0492; 0.006)$ | $\omega_b : \mathcal{N}(0.02233, 0.0004)$ | ✓ |
| Spectral index | $n_s = 0.97$ | $n_s : \mathcal{N}(0.9645; 0.08)$ | $n_s : [0.95; 0.99]$ | ✓ |
| Neutrinos | $\Sigma m_\nu = 0.06$ | $\Sigma m_\nu = 0.00\text{eV}$ | $\Sigma m_\nu = 0.06\text{eV}$ | ✓ |
| Dark Energy | $w_0 = -1$ | $w_0 : \mathcal{N}(-1.0; 0.8)$ | $w_0 = -1$ | ✓ |
| | $w_a = 0$ | $w_a : \mathcal{N}(0.0; 2.0)$ | $w_a = 0$ | ✓ |
| Astrophysical systematic models and priors: | | | | |
| Intrinsic Alignments | NLA-z | NLA+ | NLA-z | |
| | $A_{\text{IA}} = 0.4$ | $A_{\text{IA}} : \mathcal{N}(5; 3.9), \eta_{\text{IA}} : \mathcal{N}(0; 2.3)$ | $A_{\text{IA}} : [-0.6, 1.2]$ | ✗ |
| | $\eta_{\text{IA}} = 2.2$ | $\beta_{\text{IA}} : \mathcal{N}(1; 1.6), \eta_z : \mathcal{N}(0; 0.8)$ | $\eta_{\text{IA}} : [0.1, 5]$ | ✗ |
| Non-linear Model | HMCODE2020 | HALOFIT | HMCODE2020 | |
| Baryon Feedback | FLAMINGO L1_m9 | $\ell < 3000$ | Scale cuts: $K_{\text{max}} = 0.5$ | |
| | | | $\Theta_{\text{AGN}} : [7.4, 7.95]$ | ✓ |
| Neutrino Model | HMCODE2020 | N/A | HMCODE2020 | |
| Shear and Redshift Calibration: | | | | |
| σ_m^i | 0 | $ 0.013(2z_i - z_{\text{max}})/z_{\text{max}} $ | $0.002(1+z)$ | ✓ |
| σ_z^i | 0 | $0.002(1+z)$ | $0.002(1+z)$ | ✓ |
| Correlated errors? | N/A | No | Yes | |

Table 2. Cosmological parameters, astrophysical systematic models, catalogue properties and the calibration parameters: listing the input values to the mock observations and comparing our fiducial modelling and prior choices with DESC-SRD. The DESC-SRD used Gaussian priors, as this was a Fisher forecast, indicated as $\mathcal{N}(\mu; \sigma)$ with a mean μ and variance σ^2 . In this analysis we have chosen top-hat priors with the limits indicated in square brackets, and the final column indicating whether these priors are informed, ✓, or uninformed, ✗ (see Appendix C). The listed cosmological parameters are: σ_8 , the linear-theory standard deviation of matter density fluctuations in spheres of radius $8h^{-1}\text{Mpc}$ at $z = 0$; the Hubble constant, $h = H_0/(100\text{km s}^{-1}\text{Mpc}^{-1})$; the matter density, Ω_m ; the baryon density, $\omega_b = \Omega_b h^2$; the scalar spectral index, n_s ; the sum of the neutrino masses, Σm_ν .

tion measurement, m , they find a limiting systematic uncertainty at the level $\sigma_m \sim 0.002(1+z)$. This primarily arises from the sensitivity of m to changes in the distribution of intrinsic galaxy ellipticities. We choose to adopt this value for our assumed shear calibration uncertainty, including σ_m^i as an additional error to the analytical covariance described in Appendix B (see equation 37 Joachimi et al. 2021, for details). Motivated by the fact that the properties of the galaxies that give rise to this shear calibration uncertainty vary slowly between tomographic bins, we include 100% correlation in σ_m^i across the i tomographic bins. This approach is equivalent to marginalising over a single free m parameter and scaling it by fixed σ_m^i values, such that all the effective m values are 100% correlated (Asgari et al. 2021).

Our choice is optimistic compared to the shear calibration requirements set by DESC-SRD, suggesting that shear mea-

surement will not be the limiting systematic for LSST cosmic shear. It is also pessimistic compared to the accuracy forecasted for the DESC-adopted *Metadetection* technique (Sheldon et al. 2020). Using a deconvolution approach to account for noise-, model-, and detection-related bias, combined with deep data from the LSST Deep Drilling Fields, this method has been shown to deliver a shear accuracy that is better than $\sigma_m < 0.001$ (Zhang et al. 2023a; Sheldon et al. 2023). We note that this high level of accuracy is expected to degrade, however, when redshift-dependent blending is included in the forecast analysis.

2.2. Baryon Feedback

2.2.1. Building mock data using FLAMINGO

We include the suppression due to baryon feedback in our mock data vector, using the FLAMINGO hydrodynamical simulations (Schaye et al. 2023). In this suite the four parameters governing the sub-grid physics of the stellar and AGN feedback mechanisms are pre-defined to ensure the observed cluster gas fraction and the stellar mass function can be re-produced within the measurement uncertainty (Kugel et al. 2023). Assuming that the observational constraints on the hot gas content of galaxy clusters inferred from X-ray observations are not subject to selection effects or unrecognised biases, the use of FLAMINGO provides a realistic range of input feedback models for our study.

Schaye et al. (2023) simulate eleven different observationally-consistent combinations of the sub-grid parameter set, with corresponding gravity-only simulations. For our fiducial mock we adopt the fiducial FLAMINGO simulation ‘L1_m9’, a 1 Gpc intermediate resolution simulation which provides the closest match to the calibration observables (stellar mass function and cluster gas fraction) whilst also recovering the non-calibration observables (e.g. cosmic star formation history; galaxy size and metallicity; X-ray and SZ cluster scaling relations). Using measurements of the three-dimensional matter power spectrum, $P_{\text{mm}}(k, z)$ (Schaller et al. 2025), we take the ratio between the ‘L1_m9’ hydrodynamical simulation and the corresponding gravity-only simulation as our feedback suppression model. This ratio is then applied to the gravity-only non-linear matter power spectrum, generated using HMCODE2020, to mitigate the noise in the FLAMINGO realisations. We then produce predictions for the simulated C_ℓ cosmic shear power spectrum (see Appendix A). Analysing the wide range of alternative FLAMINGO simulations, which also reliably reproduce the range of different observations, we find that the ‘fgas+2 σ ’ and ‘Jet_fgas-4 σ ’⁵ scenarios induce the weakest and strongest suppression respectively, in terms of C_ℓ (see table 1 of Schaye et al. 2023, for details of the sub-grid physics of each scenario). We use the ‘fgas+2 σ ’ and ‘Jet_fgas-4 σ ’ FLAMINGO models as input to our mocks when testing the sensitivity of our analysis to weak and strong feedback scenarios.

Figure 1 shows the suppression of the cosmic shear matter power spectrum, $C_\ell^{\text{with baryons}}/C_\ell^{\text{gravity only}}$, for our fiducial mock and the weakest and strongest extremes from the FLAMINGO suite. Each box corresponds to the cosmic shear power spectrum suppression for a given pair of tomographic bins, with the auto-correlation shown on the diagonal. The lower-left corner plot shows the DESC-SRD-adopted range of scales with $20 \leq \ell \leq 3000$, where the feedback suppression can be as strong as $\sim 20\%$.

2.2.2. Scale Cuts

In this analysis we combine two approaches to mitigate our uncertainty on the impact of baryon feedback. We introduce scale cuts to remove data on highly non-linear scales and include nuisance parameters to model our uncertainty on the impact of baryon feedback on the remaining scales. These two approaches follow similar methodology applied in previous weak lensing analyses: in the DES-Y6 analysis scale cuts were applied to mitigate the impact of baryon feedback (Sanchez-Cid et al. 2026), whereas HSC-Y3 and KiDS-Legacy chose to include smaller scales and marginalise over their uncertainty on the strength of the baryon feedback using HMCODE2020 (Dalal et al. 2023;

⁵ The FLAMINGO jet model is additionally interesting as the baryonic suppression curve has a different shape compared to the other FLAMINGO simulations, (Cosmo-)OWLS and BAHAMAS, yielding a stronger suppression on large physical scales for a fixed cluster gas fraction (Schaye et al. 2023).

Wright et al. 2025b).

Starting with the scale cut definition, Figure 1 demonstrates that any optimised strategy will require redshift dependence, applying more conservative ℓ -cuts to the lower redshift bins. We therefore define a set of scale cuts, denoted⁶ $K_{\text{max}} = [0.1, 0.3, 0.4, 0.5, 0.6, 0.7, 1.0]$, where data in the tomographic bin combination ij is included when $\ell < \ell_{\text{max}}^{ij}$, with

$$\ell_{\text{max}}^{ij} = K_{\text{max}} \chi^{ij}. \quad (1)$$

Here the minimum co-moving distance $\chi^{ij} = \min[\chi(\bar{z}_i), \chi(\bar{z}_j)]$, where \bar{z}_i is the median redshift of the tomographic redshift bin i . For alternative methods to define scale cuts see Gu et al. (2025); Piccirilli et al. (2025); Zanoletti & Leonard (2025); Truttero et al. (2025); Robertson & Hall (2025). Our $K_{\text{max}} = [0.1, 0.5, 1]$ selection is shown in the lower-left corner plot of Figure 1 as the dashed grey vertical lines, with the corresponding ℓ_{max} for each tomographic bin tabulated in Appendix F.2. In the top-right corner plot we zoom into the $K_{\text{max}} = 0.5$ limited range of scales that are used for our fiducial analysis configuration (see Section 3.1).

2.2.3. Fiducial analysis with HMCODE2020

For our fiducial analysis we adopt HMCODE2020 to model the non-linear matter power spectrum (Mead et al. 2021), including the free parameter Θ_{AGN} to modulate the strength of the baryon feedback suppression⁷. There are a range of observational constraints on this parameterisation of baryon feedback, with Tröster et al. (2022) using a cross-correlation analysis of weak lensing and the thermal SZ effect finding $\Theta_{\text{AGN}} = 7.96_{-0.48}^{+0.2}$ and Ferreira et al. (2024) using the cross-correlation between cosmic shear from DES-Y3 with ROSAT X-ray data (hereafter DESxROSAT) to constrain $\Theta_{\text{AGN}} = 7.998 \pm 0.008$. These studies highlight the opportunity to use external data to set informative priors on baryon feedback models in cosmic shear. Alternatively, we can look to simulations to define an informed prior based on the Θ_{AGN} range (or any other baryon feedback parameterisation) for a given suite of simulations.

In this analysis we consider three different priors for Θ_{AGN} , shown as shaded regions in Figure 1, along with a gravity-only analysis where we use HMCODE2020 with the no feedback option. For an ‘uninformed’ prior⁸ we use a top hat $\Theta_{\text{AGN}} \in [6.5, 9.36]$ with the lower bound defined using the 1σ lower limit of the gravity-only fit, and the upper bound defined as $+7\sigma$ from the Tröster et al. (2022) constraint. The FLAMINGO-informed prior is defined by the values of $\Theta_{\text{AGN}} \in [7.4, 7.95]$ that span the full FLAMINGO range, encompassing the ‘strong’ and ‘weak’ versions of our mock data vector shown as the dashed lines in Figure 1. Finally, for the DESxROSAT observation-informed Gaussian prior with $\Theta_{\text{AGN}} \in \mathcal{N}(7.694; 0.008)$, the width is taken

⁶ We use the notation K_{max} to signify the relationship to a selection in k -space. If the galaxies in the two tomographic bins of interest were all located at a single redshift, then our defined ℓ_{max} cut would be equivalent to a k -cut at $k = K_{\text{max}}$. With the reality of broad redshift distributions, however, the projected cosmic shear signal at each ℓ -scale contains input from the underlying matter power spectrum over a wide range of k -scales. As such the K_{max} selection is only an indication of the k -scale contribution.

⁷ Θ_{AGN} is an internal parameter of HMCODE2020, related to the AGN heating parameter in the BAHAMAS simulations as $\Theta_{\text{AGN}} = \log_{10}(\Delta T_{\text{heat}}/\text{K})$. Six parameters simultaneously vary within HMCODE2020’s halo model in order to recover the BAHAMAS-predicted suppression for a range of ΔT_{heat} at percent-level accuracy. We note that any constraint on Θ_{AGN} has no physical meaning about the temperature of the AGN and that the functional form of the baryon feedback suppression predicted by HMCODE2020 does not match the FLAMINGO results precisely, as seen in Figure 1.

⁸ We note that the lower-limit of this prior is only uninformative in a cosmic shear analysis of the full ℓ -range shown in the lower right corner plot of Figure 1.

from [Ferreira et al. \(2024\)](#), with the central value chosen to be the best-fit value to the fiducial mock when all other parameters are fixed to the truth.

For our fiducial HMCODE2020 analysis we choose to use the FLAMINGO-informed prior, presenting results for the other two priors to quantify our sensitivity to this choice. The hydrodynamical simulations are unable to recover key observables outwith this range making our uninformative prior arguably over-conservative. In contrast the DESxROSAT constraints are likely over-optimistic since they derive from an analysis that assumes a fixed cosmology and metallicity value for the intra-cluster medium without accounting for the uncertain contribution to the signal from unresolved clustered X-ray AGN. The use of external observations like DESxROSAT, will likely be central to exploiting future cosmic shear observations, but given the complex astrophysical modelling that is required to interpret any ‘mass-gas’ cross-correlation data (see for example [Mead et al. 2020](#)), the level of confidence in this type of constraint will likely be debated.

There are many alternative approaches to using HMCODE2020 to model baryon feedback including: calibrated baryonification models (see for example [Bigwood et al. 2025a](#)), updated hydrodynamical simulation-informed halo models (see the [van Daalen et al. 2026](#), ‘resummation model’), along with emulators, some of which are created using machine learning techniques ([Kammerer et al. 2025](#); [Lin et al. 2025](#)). In this analysis, we choose an emulator-based alternative to HMCODE2020, modelling the impact of baryons using the SP(κ) model⁹ ([Salcido et al. 2023](#)). SP(κ) is trained on the ANTILLES suite of 400 hydrodynamical simulations that cover a wide range of stellar and AGN efficiencies, providing a diverse and flexible emulator model. One of the key strengths of this model, compared to HMCODE2020, is that the free parameters are tied to the variation of the baryon fraction as a function of halo mass $f_b(M_{\text{halo}})$. In principle, this function can be directly constrained with observations, in contrast to sub-grid feedback parameters such as Θ_{AGN} . [Salcido et al. \(2023\)](#) show that SP(κ) can recover the ANTILLES matter power spectra to a precision of 2% to $k < 10h\text{Mpc}^{-1}$.

2.2.4. Alternative analysis with SP(κ)

We use the most flexible redshift-dependent double power-law version of SP(κ) to marginalise over our uncertainty on baryon feedback. This SP(κ) version models $f_b(M_{\text{halo}})$ using four free parameters: the amplitude, ϵ ; two power-law slopes at low mass, α , and high mass, β ; a redshift dependence, γ . Here we mirror the approach of our fiducial HMCODE2020 analysis by setting informative top hat priors on these nuisance parameters, defined to span the range of the FLAMINGO simulations: $\epsilon \in [0.24, 0.35]$, $\alpha \in [-0.12, 0.34]$, $\beta \in [-0.74, 0.77]$, $\gamma \in [1.02, 1.20]$. These parameter ranges are within the ANTILLES training sample, with the exception of the redshift dependence parameter γ . Compared to ANTILLES, the FLAMINGO simulations display stronger redshift evolution.

One important caveat to note is that our analysis is underpinned by three related hydrodynamical simulations. With the exception of the jet model used in our ‘strong’ baryon mock, BAHAMAS (used to calibrate HMCODE2020), ANTILLES (used to train SP(κ)) and FLAMINGO (used to create our mocks and baryon feedback priors) derive from a similar family of models. The agreement found between these suites can therefore not be viewed as independent confirmation that the power spectra response considered in this analysis is broad enough to cover the full impact and scale-

dependence of baryon feedback on cosmic shear.

2.3. Intrinsic Galaxy Alignment

Galaxies evolve within dark matter haloes that interact with the large-scale matter distribution via gravity. Through these interactions, the underlying tidal field coherently aligns neighbouring galaxies, which we refer to as intrinsic galaxy alignment. In practice, the observed correlations between galaxy orientations combine the lensing effect of matter with the contribution from intrinsic alignments, which therefore needs to be accounted for when modelling the cosmic shear signal. Direct observations of the intrinsic alignment of galaxies are wide-ranging (see [Johnston et al. 2021](#), and references therein). Luminous red galaxies are found to exhibit a strong alignment with their local density field (e.g. [Mandelbaum et al. 2006](#)). Satellite galaxies align radially towards their central galaxy (e.g. [Georgiou et al. 2019](#)). For blue field galaxies, however, an alignment signal has yet to be detected (e.g. [Siegel et al. 2025a](#)). Unfortunately, these galaxy type-specific constraints from the literature cannot be directly incorporated in our analysis as, for a magnitude-limited cosmic shear survey like LSST, each tomographic bin will contain a different fraction of red-blue and central-satellite galaxies.

In this analysis we choose to adopt the redshift-dependent non-linear linear alignment model (NLA-z, Equation A7, [Bridle & King 2007](#); [Joachimi et al. 2011](#)) following the recommendation of [Fortuna et al. \(2021\)](#). They model the intrinsic alignment of an evolving galaxy sample using a halo model to combine constraints on galaxy type-specific alignment to predict the overall IA contamination for a Stage IV survey. By running a cosmological analysis of halo model IA-contaminated cosmic shear signals, whilst adopting the NLA-z model in their analysis framework, they determine a set of effective NLA-z parameters. The biggest uncertainty in the IA halo model arises from the uncertainty in the luminosity dependence of the red galaxy alignment. [Fortuna et al. \(2021\)](#) present parameters using a simple power-law in luminosity ($A_{\text{IA}} = 0.16 \pm 0.02$ and $\eta_{\text{IA}} = 2.91 \pm 0.70$) and a broken power-law ($A_{\text{IA}} = 0.42 \pm 0.02$ and $\eta_{\text{IA}} = 2.21 \pm 0.22$). For a Stage IV cosmic shear analysis where the underlying truth is given by an IA halo model with the alignment amplitudes determined from observations, they conclude that the adoption of an NLA-z model would not introduce a significant bias in the cosmological parameter constraints. We therefore use the two-parameter NLA-z model in our fiducial analysis with uninformative top-hat priors $A_{\text{IA}} : [-0.6, 1.2]$ and $\eta_{\text{IA}} = [0.1, 5.0]$. The edges of these priors represent $\pm 7\mathcal{D}$ about the mid-point of the simple and broken power-law constraints from [Fortuna et al. \(2021\)](#), with \mathcal{D} defined as the difference between the two results.

It has been argued that the NLA-z intrinsic alignment model is ad hoc, and we therefore include an alternative analysis utilising the Tidal Alignment and Tidal Torquing model (TATT, see equations 37-39 of [Blazek et al. 2019](#), for the intrinsic alignment power spectra). This five-parameter TATT model combines a linear alignment model with a tidal torquing alignment mechanism and a density weighting term.

2.4. Posterior Summary Statistics and Projection Effects

In this cosmic shear analysis we define our metric of success based on the accurate recovery of the most constrained cosmological parameter, S_8 . There are several summary statistics that could be employed when quoting parameter constraints, with the maximum or mean marginal distribution most often reported alongside a corresponding credible interval. It is well known, however, that these two summary

⁹ SP(κ): github.com/jemme07/pyspk

statistics do not always peak at the true parameter value, nor does the one-dimensional credible interval necessarily encompass it, as a result of projection effects (see appendix C.3 of [DK23](#), and references therein). A prior space that is asymmetric about the truth can lead to offsets between the peak of the marginalised posterior and the MAP (maximum a posteriori), when sampling over a multi-dimensional parameter space with non-linear degeneracies between constrained and unconstrained parameters.

To date, studies have mainly circumvented this issue of ‘projection bias’ by measuring relative offsets in the mean marginal between a ‘truth’ analysis, where the analysis framework perfectly matches the input noise-free mock, and a series of robustness ‘test’ analyses where different aspects of the framework are varied. Success is declared when the ‘test’ results match the ‘truth’ results, rather than the input set of cosmological parameters. We adopt this approach with a key modification introduced by [DeRose et al. \(2022\)](#); [Blake et al. \(2025\)](#): as projection effects depend on the choice of priors, scale cuts and the baryon feedback strength, a bespoke ‘truth’ analysis must be created to match each ‘test’ case. For example, when investigating the accurate recovery of cosmological parameters in the case of strong baryon feedback, our ‘test’ case will use HMCODE2020 or SP(K) to analyse a mock data vector created with the ‘Jet_fgas-4 σ ’ FLAMINGO model. Our matching HMCODE2020 ‘truth’ case will analyse a mock data vector created with HMCODE2020 where $\Theta_{\text{AGN}} = 7.931$. This value of Θ_{AGN} is the best-fitting HMCODE2020 model to the ‘Jet_fgas-4 σ ’ case, when all other parameters are fixed to the input values listed in Table 2. Our matching SP(K) ‘truth’ case will analyse a different but similar mock data vector created with SP(K) (see Appendix E for details). The mean marginal S_8 from the bespoke ‘truth’ analysis determines the level of ‘projection bias’ for each case. The offset in S_8 relative to the matching ‘test’ result then determines the accuracy of that analysis.

Our threshold for success is set at $\Delta S_8 = |S_8^{\text{truth}} - S_8^{\text{test}}| < 0.5\sigma$ where S_8^x is the mean marginal estimate from the ‘truth’ and ‘test’ chains, with σ defined as the 68% credible interval estimated from the ‘test’ chain. We recognise that this is a relatively high threshold compared to related studies from pre-cursor surveys who defined an accurate S_8 recovery to be within 0.1σ of the truth (see for example [Joachimi et al. 2021](#)), or within $0.3\sigma_{2D}$ where the offset is determined in the joint 2D (S_8, Ω_m) plane (see for example [Krause et al. 2021](#)). In the LSST case, where our high statistical power leads to very tight S_8 constraints, we find it necessary to consider a higher systematic error budget.

3. RESULTS

We present our forecast Λ CDM cosmic shear constraints for the parameters S_8 , Ω_m , A_{IA} and η_{IA} in Figure 2. Our fiducial analysis can be compared to variants of this configuration. Throughout this analysis we primarily focus on the S_8 parameter, for which our target accuracy is to recover the truth value within 0.5σ . In Section 3.1 we define our fiducial pipeline configuration for mitigating the impact of baryon feedback. In Section 3.2 we validate the robustness of our analysis to ‘stronger’ and ‘weaker’ feedback scenarios, also investigating the alternative SP(K) method for modelling baryon feedback. We consider degrading the photometric redshift calibration precision for data at Y10 depth, quantifying the impact this has on our cosmological constraints in Section 3.3. In Section 3.4 we consider the impact of our IA model and finally in Section 3.5 we consider our Λ CDM forecasts in the wider context of constraining w_0w_a CDM with multiple probes.

3.1. Defining the fiducial Y1 analysis

The DESC-SRD fiducial cosmic shear analysis adopts a scale cut of $\ell < 3000$ to mitigate against the bias introduced from the uncertain impact of baryon feedback in a w_0w_a CDM cosmology. In Figure 3 we compare the LSST Y1 cosmic shear constraints on S_8 and Ω_m for a ‘scale cut only’ flat Λ CDM analysis, progressively removing small-scale information with redshift-dependent scale cuts that range from $K_{\text{max}} = 1$ (an average $\ell_{\text{max}} \sim 1400$) to $K_{\text{max}} = 0.1$ (an average $\ell_{\text{max}} \sim 140$, see Appendix F.2). The unacceptable 1.8σ bias recovered for the S_8 parameter with a $K_{\text{max}} = 1$ scale cut can be reduced to essentially zero bias by reducing K_{max} to 0.1. This bias reduction comes at a cost, however, tripling the error on S_8 compared to the $K_{\text{max}} = 1$, recovering a value for S_8 that is hardly more constraining than existing results from [DK23](#). As the cosmological model simulated for our mock data vector adopts the most likely baryon feedback model from the FLAMINGO simulation, these results are not a ‘worst case scenario’. We agree with the conclusion of previous studies that a scale cut-only analysis is not a viable approach.

For our fiducial analysis we use HMCODE2020 to account for baryon feedback, marginalising over our uncertainty using a single parameter Θ_{AGN} (see Section 2.2.1). Figure 4 and Table 3 compare the recovered constraints on S_8 for a range of K_{max} scale cuts and the three different Θ_{AGN} priors, in addition to the ‘scale cut only’ analysis shown in Figure 3.

For the uninformative prior with $\Theta_{\text{AGN}} \in [6.5, 9.36]$, we meet our S_8 accuracy target for all tested scale cuts, but the use of this wide prior significantly impacts our precision. As shown in Figure 1 and the middle panel of Figure 4, this wide prior is effectively applying a scale cut by removing all information at high- ℓ . The precision on S_8 when using an uninformative prior is similar to a scale cut only analysis with $K_{\text{max}} \sim 0.2$ ($\ell_{\text{max}} \sim 300$), roughly doubling the error on S_8 compared to the ‘scale cut only’ $K_{\text{max}} = 1.0$ scenario shown in Figure 3.

The use of a highly constraining external prior with $\Theta_{\text{AGN}} \in \mathcal{N}(7.694; 0.008)$ (as motivated by [Ferreira et al. 2024](#)), allows us to recover most of the precision afforded by a ‘scale-cut only’ analysis. Note that only the width of this Gaussian prior is based on [Ferreira et al. \(2024\)](#) with the centre chosen to match the best fit value of Θ_{AGN} from an all-scale analysis of our fiducial FLAMINGO mock, when all other parameters are fixed. Unfortunately this constrained analysis is biased, however, only meeting our threshold criteria that $\Delta S_8 < 0.5\sigma$ for $K_{\text{max}} < 0.4$ ($\ell_{\text{max}} \sim 550$). As such it demonstrates the challenges of using tight external constraints on baryon feedback models in cases where the functional form of the model (e.g. HMCODE2020) is an imperfect reflection of the underlying truth (which in our case is the L1_m9 FLAMINGO simulation). As the physics of baryon feedback is most uncertain at high- k , it is plausible that a real-world analysis will also feature a mismatch, a model misspecification, on these scales. Our approach of using HMCODE2020 for our forecast is arguably more realistic than one where the analysis model has been trained to perfectly replicate the baryon feedback suppression input to the mock.

For our fiducial analysis set-up we chose a compromise position of adopting a FLAMINGO-based informative prior with $\Theta_{\text{AGN}} \in [7.4, 7.95]$, reflecting the fact that we do have some knowledge about the range of plausible feedback scenarios, even if we do not yet know the fine details. With this prior range we meet our accuracy target for scale cuts $K_{\text{max}} < 0.5$ ($\ell_{\text{max}} \sim 700$). This choice affords us a modest 20% improvement in S_8 -constraining power, compared to the corresponding analysis with the uninformative prior.

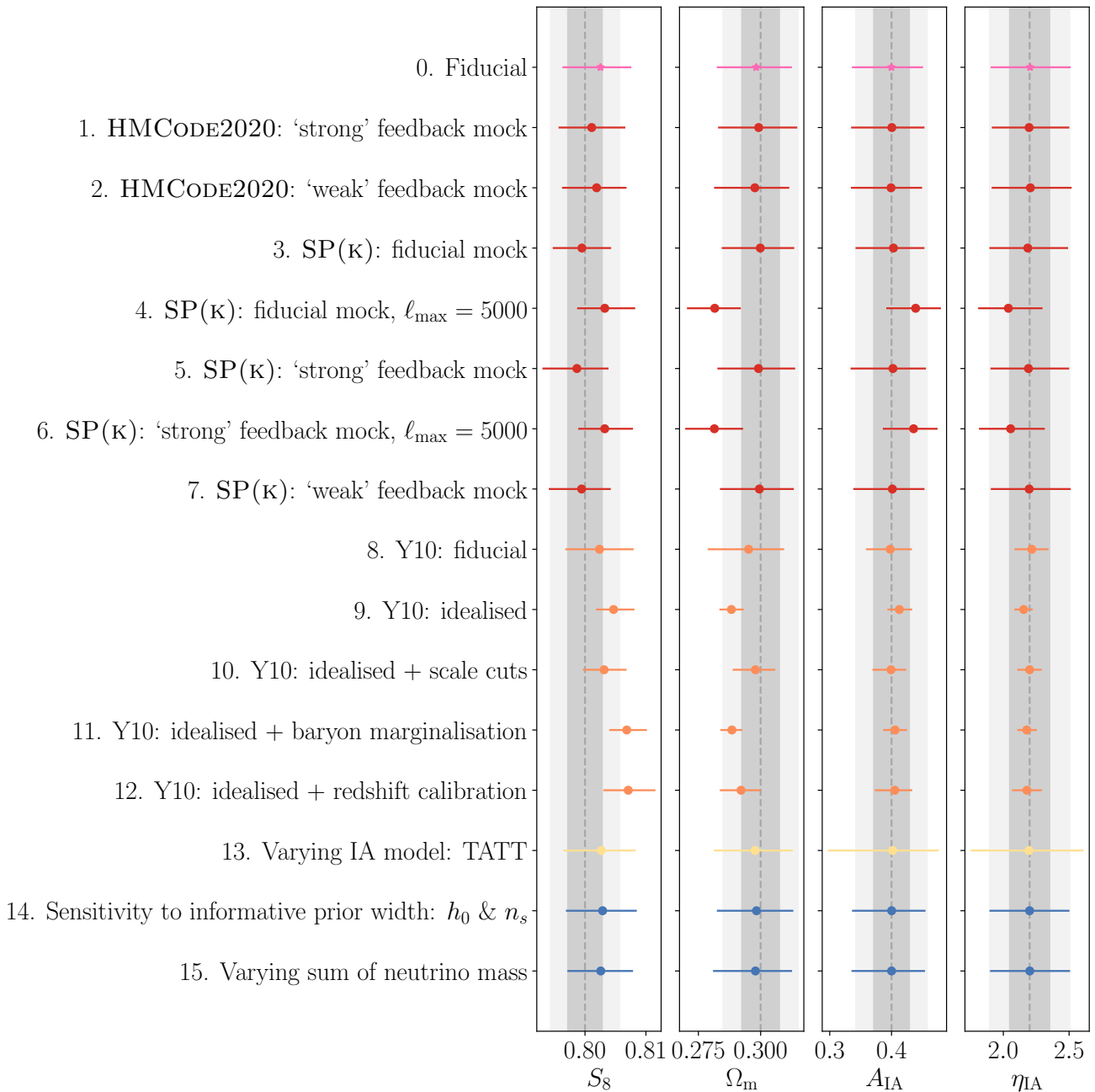


Figure 2. LSST Λ CDM cosmic shear forecasts for S_8 , Ω_m and the NLA- z intrinsic alignment parameters A_{IA} and η_{IA} , showing the mean marginal and 68% credible interval. Our Y1 fiducial analysis configuration is shown at the top in pink, with each row that follows presenting a series of variant analyses as detailed in the text. With the exception of the variants noting the use of a ‘weak’ or ‘strong’ feedback mock, we incorporate baryon feedback using the fiducial FLAMINGO model shown in Figure 1. Aside from variants noted as using scales up to an $\ell_{\max} = 5000$, we apply a scale cut of $K_{\max} = 0.5$. The dark grey region provides an indication of our target accuracy of $\pm 0.5\sigma$ uncertainty, about the ‘truth’ (shown dashed), where σ is the 68% credible interval from our fiducial Y1 analysis. Note that here we show $S_8 = S_8^{\text{input}} + \Delta S_8$, and the equivalent for the other parameters. The input values are listed in Table 2, with the Δ offsets determined from the difference between the mean marginal estimates from the ‘truth’ and ‘test’ mock analyses (see Section 2.4 for details). For the purpose of this figure, the 0.5σ -width is set to the constraining power of our fiducial analysis. The light grey region corresponds to $\pm 1\sigma$ uncertainty. Rows 1-7 review the robustness of the Y1 HMCODE2020 fiducial pipeline, and an alternative SP(κ)-based analysis, to weaker and stronger baryon feedback (Section 3.2). Rows 8-12 assess the impact of systematics mitigation strategies for Y10 (Section 3.3). Row 13 adopts the alternative TATT intrinsic alignment model for Y1 (Section 3.4). Rows 14-15 vary the Y1 set of cosmological parameters and priors (Appendix C). The constraints on S_8 are tabulated in Appendix F.2.

The S_8 error is, however, a factor of 1.5 larger than the highest precision ‘scale-cut only’ biased constraints.

Our adopted fiducial scale cut at $K_{\max} < 0.5$ ($\ell_{\max} \sim 700$) is significantly different from the original DESC-SRD gravity-only forecast which proposed to analyse the cosmic shear power spectra to $\ell < 3000$. Inspecting the middle-panel of Figure 4, however, we see there is little information gain for S_8 beyond $K_{\max} = 0.6$ ($\ell_{\max} \sim 800$), when considering the highest precision gravity-only analysis. Taking a pragmatic approach of removing scales that are challenging to model is therefore not as drastic an action as it first

appears.

3.2. Varying the baryon feedback strength and model

We quantify the sensitivity of our cosmic shear analysis to changes in the input baryon feedback strength by analysing the alternative ‘weak’ and ‘strong’ mock data shown in Figure 1. Using our fiducial analysis set-up, a FLAMINGO-based informative prior on Θ_{AGN} with a scale cut of $K_{\max} = 0.5$, we recover S_8 within our target accuracy of $< 0.5\sigma$, for both extremes in feedback strength.

In Figure 5 we compare the ‘truth’ and ‘test’ marginal constraints for the analysis of mock ‘weak’ and ‘strong’

| Baryon Prior | Scale Cut | ‘Test’ Mock | | ‘Truth’ Mock | | Bias | | |
|---------------|------------------------|---------------------------|-------------------------|---------------------------|-------------------------|---------------|--|------------------------------|
| | | S_8 | $S_8 - S_8^{\text{in}}$ | S_8 | $S_8 - S_8^{\text{in}}$ | ΔS_8 | $\sigma_{\text{Test}}/\sigma_{\text{Truth}}$ | $\sigma/\sigma_{\text{Fid}}$ |
| FLAMINGO | $K_{\text{max}} = 0.5$ | $0.802^{+0.005}_{-0.006}$ | 0.31σ | $0.799^{+0.005}_{-0.006}$ | -0.14σ | 0.45σ | 1.04 | 1.00 |
| FLAMINGO | $K_{\text{max}} = 1.0$ | $0.803^{+0.005}_{-0.005}$ | 0.52σ | $0.799^{+0.005}_{-0.006}$ | -0.17σ | 0.69σ | 0.91 | 0.92 |
| FLAMINGO | $K_{\text{max}} = 0.5$ | $0.802^{+0.005}_{-0.006}$ | 0.31σ | $0.799^{+0.005}_{-0.006}$ | -0.14σ | 0.45σ | 1.04 | 1.00 |
| FLAMINGO | $K_{\text{max}} = 0.1$ | $0.800^{+0.014}_{-0.012}$ | 0.03σ | $0.800^{+0.013}_{-0.012}$ | -0.03σ | 0.06σ | 1.03 | 2.29 |
| DM only | $K_{\text{max}} = 1.0$ | $0.793^{+0.004}_{-0.004}$ | -1.91σ | $0.800^{+0.004}_{-0.004}$ | -0.10σ | -1.82σ | 0.97 | 0.69 |
| DM only | $K_{\text{max}} = 0.5$ | $0.795^{+0.005}_{-0.004}$ | -1.01σ | $0.800^{+0.005}_{-0.005}$ | -0.08σ | -0.93σ | 1.00 | 0.82 |
| DM only | $K_{\text{max}} = 0.1$ | $0.799^{+0.013}_{-0.012}$ | -0.05σ | $0.800^{+0.012}_{-0.013}$ | -0.02σ | -0.03σ | 1.00 | 2.15 |
| Uninformative | $K_{\text{max}} = 1.0$ | $0.801^{+0.006}_{-0.007}$ | 0.19σ | $0.799^{+0.006}_{-0.006}$ | -0.23σ | 0.42σ | 1.06 | 1.13 |
| Uninformative | $K_{\text{max}} = 0.5$ | $0.799^{+0.005}_{-0.008}$ | -0.17σ | $0.797^{+0.006}_{-0.009}$ | -0.45σ | 0.28σ | 0.93 | 1.19 |
| Uninformative | $K_{\text{max}} = 0.1$ | $0.802^{+0.012}_{-0.013}$ | 0.18σ | $0.802^{+0.013}_{-0.014}$ | 0.12σ | 0.06σ | 0.95 | 2.27 |
| DESxROSAT | $K_{\text{max}} = 1.0$ | $0.802^{+0.005}_{-0.004}$ | 0.52σ | $0.799^{+0.004}_{-0.004}$ | -0.18σ | 0.69σ | 1.10 | 0.77 |
| DESxROSAT | $K_{\text{max}} = 0.5$ | $0.802^{+0.005}_{-0.005}$ | 0.44σ | $0.799^{+0.005}_{-0.004}$ | -0.15σ | 0.60σ | 1.02 | 0.85 |
| DESxROSAT | $K_{\text{max}} = 0.1$ | $0.800^{+0.013}_{-0.012}$ | -0.002σ | $0.799^{+0.012}_{-0.013}$ | -0.05σ | 0.04σ | 0.96 | 2.17 |

Table 3. LSST-Y1 Λ CDM cosmic shear forecasts for S_8 . We consider three sets of scale cuts, $K_{\text{max}} = [0.1, 0.5, 1.0]$, and three choices of prior for the HMCODE2020 baryon feedback parameter: Uninformative, $\Theta_{\text{AGN}} \in [6.5, 9.36]$; FLAMINGO-informed, $\Theta_{\text{AGN}} \in [7.4, 7.95]$; DESxROSAT, $\Theta_{\text{AGN}} \sim \mathcal{N}(7.694; 0.008)$. Constraints from a ‘scale-cut only’ analysis, where baryon feedback is not modelled, are also tabulated (DM only). We conduct two analyses for each variant. In the ‘Truth Mock’, the input mock is created by, and analysed with, HMCODE2020. The offset from the input cosmology, $S_8 - S_8^{\text{in}}$, in this ‘truth’ case, is therefore a measure of projection bias, which varies for each analysis setup, and can be as high as -0.45σ when using uninformative priors. In the ‘Test Mock’, the mock is created by the fiducial FLAMINGO L1_m9 simulation, but analysed with HMCODE2020 (see Section 2.4 for details), creating an offset in the recovered value of S_8 which combines both model bias and projection effects. Throughout this study we remove the projection offset by reporting $\Delta S_8 = (S_8^{\text{truth}} - S_8^{\text{test}})$ as a fraction of the mean marginal 1σ error estimate. The table also compares the relative constraining power of each analysis as the ratio, $\sigma/\sigma_{\text{Fid}}$, to the fiducial $K_{\text{max}} = 0.5$ analysis reported in the top row.

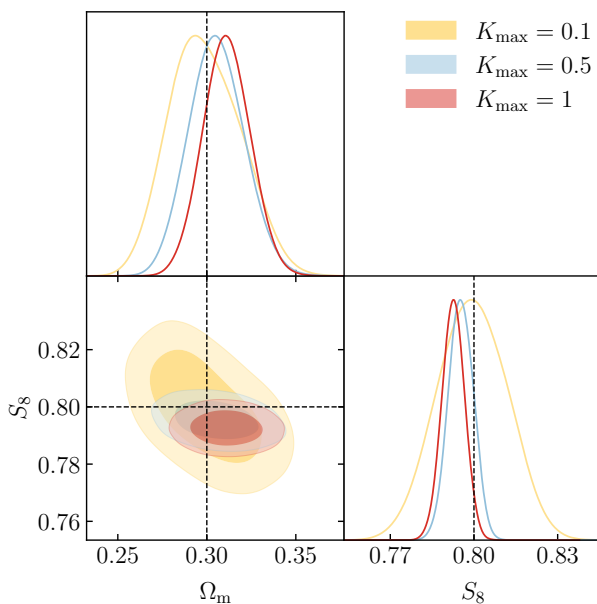


Figure 3. LSST Y1 cosmic shear forecasts on S_8 and Ω_m for a ‘scale cut only’ analysis that does not model baryon feedback. We compare three different redshift-dependent scale cuts: $K_{\text{max}} = 1$ (blue), $K_{\text{max}} = 0.5$ (red), and $K_{\text{max}} = 0.1$ (yellow) (see Appendix F.2 for how K_{max} relates to ℓ_{max} in different tomographic bins). As we remove scales, the constraining power and the bias reduce significantly. A 2σ bias on S_8 for $K_{\text{max}} = 1$ decreases to a 0.03σ offset for $K_{\text{max}} = 0.1$, with the error on S_8 tripling and becoming comparable to existing constraints from pre-cursor surveys. These results are all cases of ‘test’ analyses where the projection ‘bias’ is low at $\sim 0.1\sigma$. In this figure, and all similar contour plots that follow, the dashed black lines indicate the input cosmology (listed in Table 2), with the marginalised posterior contours showing the 68% (inner) and 95% (outer) credible intervals. The constraints on S_8 are tabulated in Table 3.

feedback LSST-Y1 cosmic shear. The mean marginal ‘test’ case results (where a FLAMINGO-based mock has been analysed using an HMCODE2020 framework) do not return the input cosmology with S_8 offset from the input value by -0.8σ and 0.6σ in the strong and weak scenarios respectively. As seen from the ‘truth’ case results, however, (where strong and weak HMCODE2020-based mocks have

been analysed using an identical HMCODE2020 framework), this offset predominantly arises from projection effects. The primary source of this ‘projection bias’ is the baryon feedback parameter Θ_{AGN} which is shown to be correlated with S_8 . When informative priors are asymmetrically distributed about the truth, the mean of the one-dimensional marginal posterior distributions for constrained parameters can differ significantly from the input values. When we account for this projection effect, we can conclude that the accuracy of our fiducial set-up is sufficiently insensitive to changes in the underlying baryon feedback mechanism.

To test the impact of our choice of HMCODE2020 as our feedback model, Figure 2 compares our fiducial analysis to an analysis that adopts SP(κ) to model the baryon feedback. Using the same $K_{\text{max}} = 0.5$ scale cut, this flexible four-parameter baryon feedback model accurately recovers the input S_8 values for the fiducial, ‘weak’ and ‘strong’ mock data vectors, with no degradation in constraining power. The constraints on S_8 for these tests are tabulated in Appendix F.2.

Boruah et al. (2024) argue that with a sufficiently accurate and flexible baryon feedback model, the application of any scale cuts is detrimental to the cosmological constraining power. Based on the highly accurate SP(κ) recovery of the FLAMINGO 3D power-spectra, we therefore conduct an SP(κ) analysis using scales to $\ell_{\text{max}} = 5000$. Analysing the full fiducial and ‘strong’ mock data vector with SP(κ), we are unable to recover S_8 at target accuracy, finding a bias of $\sim 0.7\sigma$ (after accounting for projection bias) and a $\sim 15\%$ improvement on constraining power compared to our scale cut analysis. The bias can be understood by noting that the SP(κ) emulator is limited to $k < 12h\text{Mpc}^{-1}$, and our cosmic shear C_ℓ mocks are projections of the FLAMINGO 3D power spectra to a $k_{\text{max}} = 40\text{Mpc}^{-1}$. This mismatch could be rectified with a new SP(κ) training sample. Given the marginal $\sim 15\%$ improvement in constraining power, however, we find no strong motivation to extend our analysis beyond HMCODE2020 at this time. Access to tight observational constraints on the $f_b(M_{\text{halo}})$ relationship (for exam-

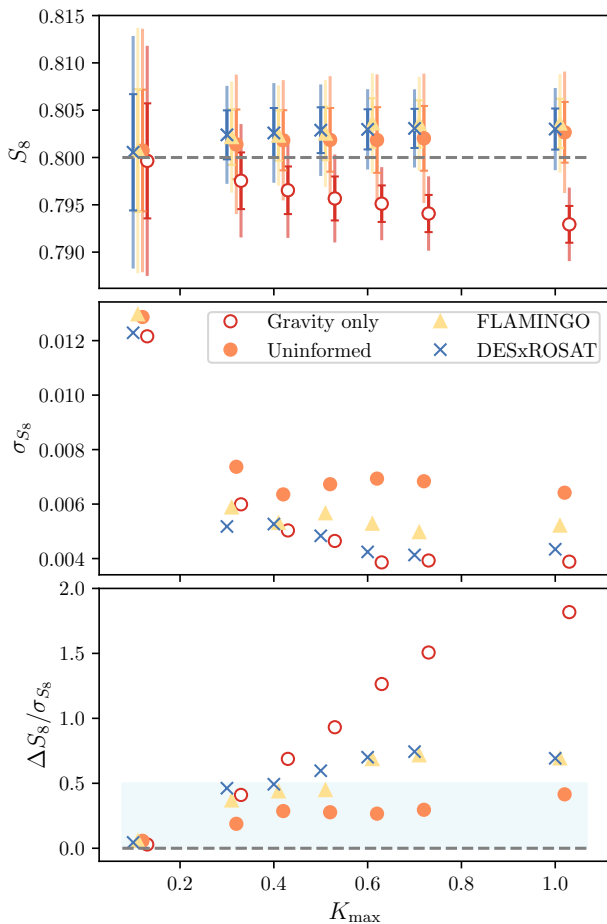


Figure 4. Comparing S_8 constraints when varying K_{\max} scale-cuts and different baryon feedback priors. Top: Mean marginal ‘test’ analysis constraints on S_8 , where the inner and outer error bars correspond to 0.5σ and 1σ respectively, and the dashed line marks the input value. The projection ‘bias’ is reported in Table 3, and can be as high as 0.4σ . Middle: 68% confidence interval error estimate for S_8 . Lower: the absolute value of the offset $\Delta S_8 = |(S_8^{\text{truth}} - S_8^{\text{est}})|$ as a fraction of the error. We define success as a result where $\Delta S_8 < 0.5\sigma$ (shaded blue). We see that a gravity-only analysis that ignores the impact of baryon feedback (red) is only unbiased when excluding all but the smallest ℓ -scales in the cosmic shear analysis. When using wide priors to marginalise over baryon feedback uncertainty (Uninformed, orange, and FLAMINGO-informed, yellow), little information is gained by increasing K_{\max} to high values. Using external information to constrain the baryon feedback (DESxROSAT, blue) returns precision at the expense of accuracy.

ple, Bigwood et al. 2024), and hence the four $\text{SP}(\kappa)$ parameters, would, however, clearly motivate the use of $\text{SP}(\kappa)$ over HMCODE2020 in the future (see also van Daalen et al. 2026).

3.3. Varying survey depth: analysing Y10

Across ten years of observations, LSST will more than double the effective source density for cosmic shear studies. In this analysis we have adopted the DESC-SRD survey parameters for Y10, assuming a survey with 14,300 square degrees of data down to a 5σ limiting magnitude of $i < 26.35$ (see Table 1 and Appendix B). This unrivalled depth, however, raises a significant issue for the precise calibration of photometric redshifts without a representative deep spectroscopic sample. To account for this challenge we increase our uncertainty on the Y10 redshift accuracy to $\delta_z^i = 0.015$, based on existing analyses that utilise an alternative cross-correlation calibration scheme (as discussed in Section 2.1). Our approach contrasts with DESC-SRD, where the systematic uncertainty requirements were set at a target level $\delta_z^i = 0.001(1 + z_i)$, highlighting the current order of magnitude difference that exists between the redshift calibration accuracy that could be accomplished for Y10 today and the

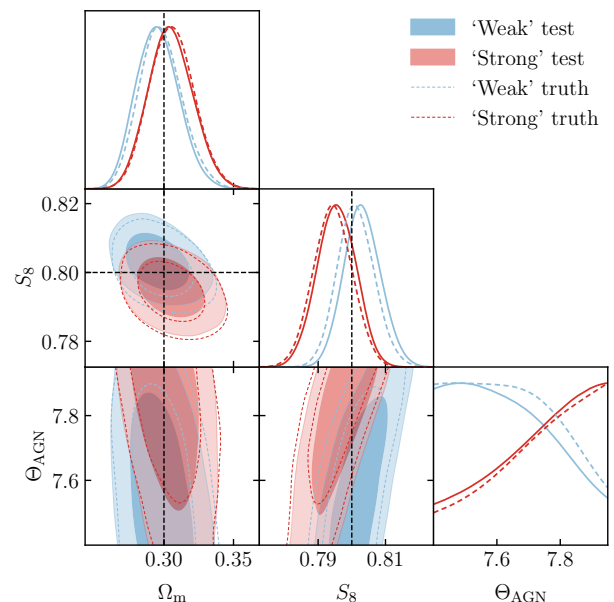


Figure 5. Varying the baryon feedback strength: comparing constraints on S_8 , Ω_m and the HMCODE2020 baryon feedback parameter Θ_{AGN} for the weakest (blue) and strongest (pink) feedback scenario from the suite of FLAMINGO simulations. The ‘truth’ cases quantify the level of ‘projection bias’ relative to the input cosmology (shown dashed). The ‘test’ cases (where the mock data doesn’t match the analysis framework) recover the matching ‘truth’ case within our target accuracy of $< 0.5\sigma$.

requirements of the future.

In Figure 6 we compare our fiducial analyses of the LSST-Y1 and LSST-Y10 mock cosmic shear measurements, finding little improvement for the Y10 S_8 and Ω_m cosmic shear constraint over Y1. The combination of redshift uncertainty, baryon feedback marginalisation and the $K_{\max} = 0.5$ scale cuts that we have adopted in our fiducial analyses gives rise to an information plateau that effectively erases the benefits of increasing the survey depth. To understand the relative impact of these three systematic mitigation strategies for Y10, we run the series of tests summarised in Table 4, with the resulting constraints in the $S_8 - \Omega_m$ plane shown in Figure 7.

We start with an ‘idealised’ case, taking the DESC-SRD the science goal requirements on the photometric redshift calibration¹⁰ of $\delta_z^i = 0.001(1 + z_i)$; using scales to $\ell_{\max} = 5000$; fixing the HMCODE2020 baryon feedback amplitude, Θ_{AGN} , at the best-fit value to the fiducial FLAMINGO model. The error on S_8 from this idealised Y10 analysis is almost halved compared to our fiducial case (see Figure 6). Taking this idealised case, we then apply each systematic mitigation strategy in turn. The error on S_8 increases by a factor of 1.1 when applying scale cuts, and by a factor of 1.4 when widening the δ_z^i prior. Marginalising over baryon feedback has little of impact on the constraining power in the absence of scale cuts.

We find that none of the Y10 idealised test cases meet our target accuracy to recover the ‘truth’ cosmology within 0.5σ , which is expected based on the corresponding Y1 analysis in Section 3.1: with HMCODE2020 we need to combine scale cuts with baryon feedback modelling to recover unbiased results. It is worth noting that the redshift calibration and baryon marginalisation case find a value for S_8 that is biased particularly high. This results from the wider priors on δ_z^i , or Θ_{AGN} , allowing the nuisance parameters to shift away from their true value in order to absorb

¹⁰ We note that an idealised cosmic shear analysis where the photometric redshift calibration matches the Y1 SOM-based case of $\delta_z^i = 0.002(1 + z_i)$ is found to hardly differ from an idealised analysis using the DESC-SRD requirement of $\delta_z^i = 0.001(1 + z_i)$.

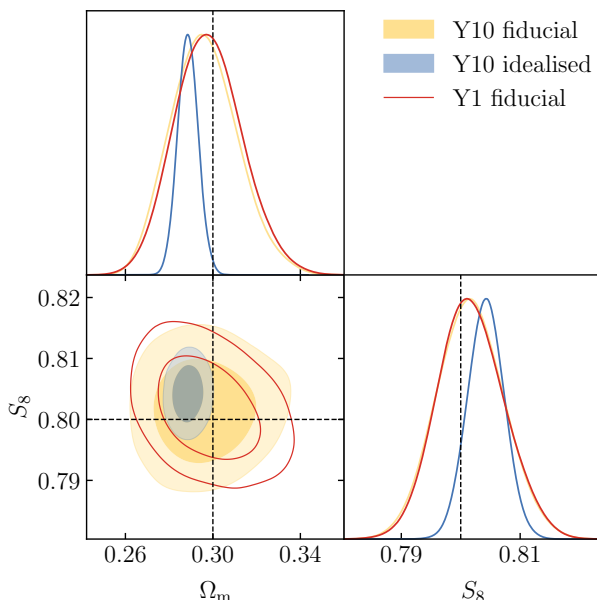


Figure 6. Comparison of fiducial analyses for LSST-Y1 (red) and LSST-Y10 (yellow) mock cosmic shear measurements, showing little improvement in constraining power for Y10 over Y1. Our Y10 baseline analysis increases the uncertainty on the redshift accuracy compared to Y1, with $\delta_z^i = 0.015$, to account for the challenges of redshift calibration with an ultra-deep survey. When adopting the idealised approach of DESC-SRD, the error on S_8 and Ω_m is roughly halved (blue).

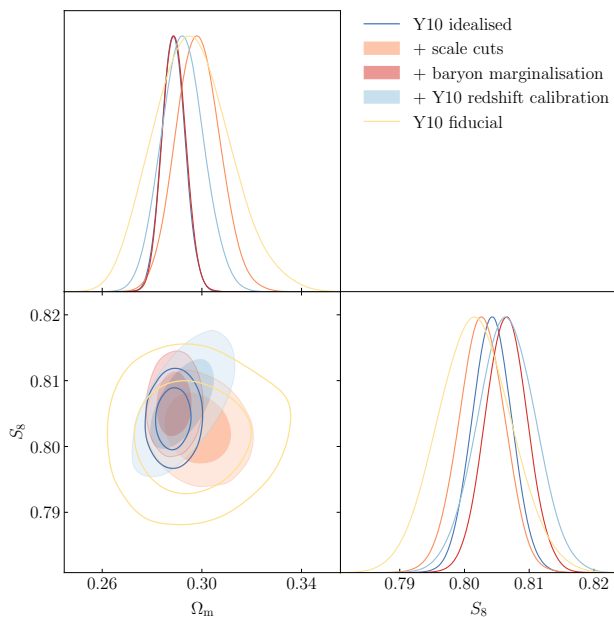


Figure 7. Comparison of the limiting factors in a Y10 cosmic shear analysis. Idealised DESC-SRD-like contours (dark blue, unfilled) are modified by the impact of $K_{\max} = 0.5$ scale cuts (orange), baryon feedback marginalisation (red) and redshift uncertainty (blue), all of which are combined in our Y10 baseline analysis (yellow unfilled). The constraints on S_8 are tabulated in Table 7.

the high- k model mismatch between HMCODE2020 and the input FLAMINGO simulation. Leonard et al. (2024) see similar behaviour when there is a mismatch between the adopted intrinsic alignment model and the input truth. This demonstrates that any degradation in the precision of the photometric redshift calibration for Y10 over Y1, will further exacerbate the issue of accounting for baryon feedback uncertainty in our cosmic shear analysis. Improved external observations to constrain these systematic uncertainties will be essential if Y10 is to realise the DESC-SRD forecasts.

3.4. Varying the intrinsic alignment model

To test the impact of our choice of the two-parameter NLA- z intrinsic galaxy alignment model, Figure 2 compares our fiducial analysis to an analysis that adopts the five-parameter TATT model (Blazek et al. 2019). We find no impact on the accuracy or precision of our cosmic shear constraints on S_8 and Ω_m from the choice of intrinsic alignment model. The full marginalised posteriors are compared in Appendix F.1.

These findings differ from a wide range of data analyses that report an error on S_8 that grows by up to $\sim 40\%$ when using TATT over NLA- z (see the discussion in section 3.3 of DK23, and references therein). It is, however, in agreement with mock data studies where the intrinsic alignment model has been simulated to match NLA- z (DK23), as is the case with this study where the three additional TATT parameters have a ‘truth’ value of zero in our mock.

For this lensing-only analysis, we choose to limit our intrinsic alignment study to this single test case as there is already a significant body of work in this area. We refer the reader to Samuroff et al. (2024) for a detailed exploration of the significant bias introduced in an LSST Y1-like NLA- z -based analysis when the true intrinsic alignment mechanism is given by an extreme TATT model. This result would nominally motivate the use of TATT as the default, but Fischbacher et al. (2023) and Leonard et al. (2024) demonstrate how without tight priors on the photometric redshift calibration uncertainty, weakly constrained TATT parameters can absorb errors in the redshift distribution leading to a bias on the derived cosmological parameters. With a ‘ $3 \times 2pt$ ’ joint lensing and galaxy clustering analysis, many of the issues related to intrinsic alignment model bias can, however, be mitigated (Leonard et al. 2024; Samuroff et al. 2024)

Euclid Collaboration et al. (2025a) have recently studied the impact of individual nuisance parameter mis-modelling problems for a combined $3 \times 2pt$ and spectroscopic clustering data vector within Λ CDM for Euclid. They predominantly find relatively mild posterior effects of around 1σ , reflecting both the calibrating effect of combining with clustering data, and the already tight prior requirements on end-stage Euclid results. They find very large ($\approx 5\sigma$) posterior biases, however, when analysing mock data generated without intrinsic alignments using a simple (NLA) model, which should subsume such a configuration. They ascribe this to prior volume effects, but the discrepancy in their located best-fit values suggests this may not be the cause. We do not find corresponding results in our cosmic shear-only analysis.

In this analysis we adopt a set of overlapping tomographic bins, each with a known 7% outlier population, adopting correlated priors for the photometric redshift calibration uncertainty δ_z^i in each bin (see Appendix B for details). In a robustness test of these choices, we find that assuming uncorrelated δ_z priors in our Y1 fiducial analysis has no impact on our parameter constraints. Removing the outlier population, and modifying the input model redshift distributions accordingly, does, however, improve the constraints on the intrinsic alignment parameters by $\sim 10\%$ for A_{IA} and $\sim 15\%$ for η_{IA} (see also Zhang et al. 2026). Despite this improved intrinsic alignment model, however, the recovered constraints on S_8 remain unchanged. For the case of a redshift distribution where the outlier population is unknown, we refer the reader to (Mill et al. 2025) and section V1.A of Boruah et al. (2024) which both forecast a significant bias in the recovered cosmological parameter constraints, if the outlier population is not known within 5% accuracy.

3.5. Joint Constraints in $w_0 - w_a$ CDM

In our analyses of both the Y1 and Y10 mock cosmic shear observations we have shown that baryon feedback

| Analysis ID | Scale Cuts | Θ_{AGN} Prior | δ_z Prior | S_8 | ΔS_8 | $\sigma/\sigma_{\text{Fid}}$ |
|--------------------------|----------------------------|-----------------------------|------------------|---------------------------|--------------|------------------------------|
| Idealised | $\ell_{\text{max}} = 5000$ | 7.694 | $0.001(1+z)$ | $0.804^{+0.003}_{-0.003}$ | 1.49σ | 1.00 |
| Baryon Marginalisation | $\ell_{\text{max}} = 5000$ | $\in [7.4, 7.95]$ | $0.001(1+z)$ | $0.806^{+0.003}_{-0.003}$ | 2.21σ | 0.98 |
| Scale cuts | $K_{\text{max}} = 0.5$ | 7.694 | $0.001(1+z)$ | $0.803^{+0.004}_{-0.003}$ | 0.87σ | 1.14 |
| Y10 Redshift Calibration | $\ell_{\text{max}} = 5000$ | 7.694 | 0.015 | $0.806^{+0.004}_{-0.004}$ | 1.66σ | 1.36 |
| Y1 fiducial | $K_{\text{max}} = 0.5$ | $\in [7.4, 7.95]$ | $0.002(1+z)$ | $0.802^{+0.005}_{-0.006}$ | 0.45σ | 1.80 |
| Y10 fiducial | $K_{\text{max}} = 0.5$ | $\in [7.4, 7.95]$ | 0.015 | $0.802^{+0.006}_{-0.006}$ | 0.42σ | 1.78 |

Table 4. To understand the comparable constraining power of Y1 and Y10 for our fiducial analysis configuration, we take an idealised Y10 case, described in the top line, and consider the impact of three systematic mitigation strategies individually. These are baryon feedback marginalisation with Θ_{AGN} , scale cuts and redshift calibration uncertainty with a prior on δ_z . Each time we change only one aspect of the pipeline set-up, relative to the idealised case. The final lines report the results of our Y1 and Y10 fiducial analyses. The right side of the table tabulates the S_8 ‘test analysis’ constraints, the bias in S_8 (including projection effects which are $\sim -0.1\sigma$ for each case), and the error on S_8 relative to the idealised case. Constraints in the S_8 - Ω_m plane are shown in Figure 7.

mitigation strategies contribute significantly to the systematic error budget. In order to recover accurate cosmological parameters, without external observations to set tight priors on the amplitude and scale-dependence of the baryon feedback mechanism, we are forced to accept a significant reduction in constraining power on the Λ CDM model. This clear result is, however, in stark contrast to the LSST forecasts of [Boruah et al. \(2024\)](#) who find that baryon feedback contributes just 1% to their total error budget. In this section we discuss how differences in methodology and success metrics lead to these contrasting conclusions.

Our cosmic shear-only Λ CDM analysis differs from [Boruah et al. \(2024\)](#) in that they analyse the impact of astrophysical systematics in a ‘ 3×2 pt’ forecast of $w_0 w_a$ CDM. Their metric of success is the composite dark energy parameter $w_p = w_0 + w_a [z_p / (1 + z_p)]$ at a pivot redshift $z_p = 0.4$. Using a flexible baryon feedback model they analyse the 3×2 pt LSST data vector, finding no need to introduce any additional scale cuts¹¹ in their analysis as w_p is recovered, for a range of input baryon feedback models, within the target accuracy of $< 0.3\sigma$.

One concern over the use of the w_p metric, is that it is insensitive to biases in other cosmological parameters. As the target dark energy constraints for LSST rely on the inclusion of additional and external probes, we consider whether a biased S_8 constraint from an inaccurate cosmic shear analysis could introduce an error in the joint dark energy constraints.

Figure 8 presents $w_0 w_a$ CDM forecasts for an analysis of our fiducial LSST-Y1 cosmic shear mock data vector, including a ‘CMB+’ prior that mimics the combined constraints from the ‘Stage-III’ CMB ([Planck Collaboration 2020](#)), baryon acoustic oscillations ([Alam et al. 2017](#)), the local distance ladder¹² ([Riess et al. 2018](#)) and type Ia supernova ([Scolnic et al. 2018](#)). We find that the addition of our Y1 fiducial cosmic shear analysis would decrease the error on S_8 , by a factor of 2.7, over Stage-III alone. Very little impact is seen for the constraint on w_0 , which improves by only a few percent in the joint analysis, but the error on w_a decreases by 16%.

Following [Boruah et al. \(2024\)](#), we conduct a joint analysis that includes cosmic shear data to an $\ell_{\text{max}} = 5000$ and marginalises over our uncertainty. In this ‘all scale’ analysis we find a significant $\sim 0.8\sigma$ bias in S_8 , as expected from Section 3.1. Importantly, however, we find that this offset in S_8 does not translate into a large biases in the dark energy parameters. The bias in the recovered w_0 and w_a

¹¹ [Boruah et al. \(2024\)](#) use real space statistics, applying a scale cut of 1 arcmin for both components of the two-point shear correlation function ξ_{\pm} .

¹² The ‘Stage-III’ prior re-produces the constraints expected from the combination of data sets, assuming there is no tension between the different probes.

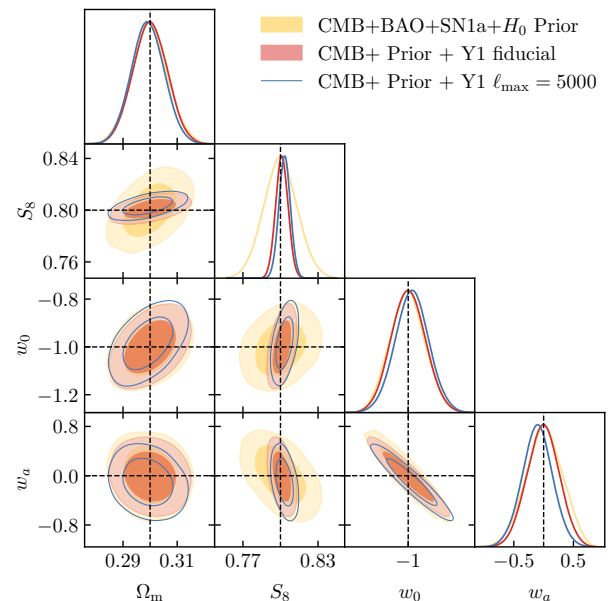


Figure 8. Comparison of constraints on Ω_m , S_8 , w_0 and w_a for our fiducial Y1 cosmic shear data vector with a ‘CMB+’ prior (yellow) that imitates combined constraints from the CMB ([Planck Collaboration 2020](#)), baryon acoustic oscillations ([Alam et al. 2017](#)), the local distance ladder ([Riess et al. 2018](#)) and Type Ia supernova ([Scolnic et al. 2018](#)). By including Y1 cosmic shear data using our fiducial analysis (red), the constraints on S_8 are improved by a factor of 2.7. We find only a slight improvement in the constraints on w_0 and w_a in a joint analysis, even when including small-scale information to an $\ell_{\text{max}} = 5000$ (blue). This motivates us to focus on S_8 constraints when setting requirements on early LSST cosmic shear analyses.

constraints in this case rise to 0.2σ and 0.4σ respectively, which is within our level of tolerance. As such we can understand the differing conclusions between this study and [Boruah et al. \(2024\)](#). The use of an imperfect baryon feedback mitigation scheme significantly impacts the S_8 constraints in a Λ CDM analysis. For the dark energy parameters in a 3×2 pt $w_0 w_a$ CDM analysis, however, the impact is relatively small. We conclude that the requirements on the accuracy of the baryon feedback model can be reduced if the goal of the analysis is to solely constrain the dark energy parameters.

4. CONCLUSIONS

Rubin and *Euclid* have been designed to deliver percent-level precision measurements of the w_0 and w_a parameters that model the evolving equation of state of dark energy. To achieve that goal though, both surveys will require additional information from the CMB observations that currently lie in mild tension with a number of existing low-redshift observables. As offsets between complementary probes could be indicative of systematic bias or ‘new

physics’, this analysis has focussed on quantifying how significant the bias could be for an LSST cosmic shear analysis in light of the wide range of feasible baryon feedback scenarios recovered from the latest FLAMINGO suite of hydrodynamical simulations (Schaye et al. 2023). In order to reduce the systematic bias on the most constrained parameter, S_8 , to below 0.5σ , we find that our fiducial analysis requires the removal of small-scale information out to a $K_{\max} = 0.5$ ($\ell_{\max} \sim 700$). This approach improves accuracy, but at a cost: the S_8 error for our unbiased fiducial analysis is almost double that of the $\sim 2\sigma$ -biased analysis where baryon feedback is ignored.

In our fiducial analysis we marginalise over the amplitude of the baryon feedback suppression to the non-linear matter power spectrum using the one-parameter HMCODE2020 model (Mead et al. 2021). This approach is arguably insufficient to model the complexity of the FLAMINGO simulations, but unfortunately our conclusion about the degradation in constraining power that arises from baryon feedback mitigation is unchanged by the adoption of the more sophisticated four-parameter SP(κ) model (Salcido et al. 2023). This flexible emulator has been trained on 400 ANTILLES hydrodynamical simulations providing an emulation of all the ANTILLES models, accurate to 2% out to $k < 10h\text{Mpc}^{-1}$. Without tight priors to inform the SP(κ) parameters, however, the marginalisation over the full ANTILLES space effectively removes most of the cosmic shear information at high- ℓ . In an ‘all-scale’ SP(κ) cosmic shear analysis, the constraints on S_8 are unchanged compared to a scale-cut SP(κ) analysis. Problematically, this flexible ‘all-scale’ SP(κ) analysis also fails to meet our target accuracy, with $\sim 0.7\sigma$ biases in the recovery of S_8 , highlighting the challenge of analysing data at the high- ℓ scales where there is significant uncertainty over the impact of baryon feedback.

We find that the use of the DESxROSAT tight prior for the baryon feedback model (Ferreira et al. 2024), reduces the error on S_8 to become comparable with the forecasts from the idealised DESC-SRD case where baryon feedback is ignored. This prior needs to be combined with an accurate scale-dependent model, however, which we currently lack. Throughout this analysis we have shown how the mild high- k mismatch between our analysis models (HMCODE2020 and SP(κ)) and our mock FLAMINGO input can be absorbed by other parameters in the cosmological analysis, leading to biased constraints on S_8 . Unfortunately the solution is not as simple as updating our analysis models to better match FLAMINGO, as recent joint X-ray-kSZ analyses have demonstrated that these state-of-the-art hydrodynamical simulations are likely incomplete, unable to fully reproduce the extended gas profiles seen in observational data (Siegel et al. 2025b). The mismatch between model and mock that we have included in this analysis therefore provides a reasonable reflection of our current uncertainty of this effect. We conclude that understanding baryon feedback must become a top priority for both *Rubin* and *Euclid*, if cosmic shear is to remain a competitive probe.

We recognise that our conclusion is at odds with the LSST forecasts from Boruah et al. (2024) who found that baryon feedback uncertainty contributes minimally to the error budget. This difference results from our two studies addressing two different questions. In this analysis we have focused on forecasts for Λ CDM, motivated by the current drive in the cosmological community to understand the tensions that exist between current data sets. In contrast Boruah et al. (2024) ask: how accurately will an LSST $3 \times 2\text{pt}$ analysis constrain dark energy? In our joint analysis forecast of LSST-Y1 cosmic shear with the CMB and other external probes, we also conclude that the baryon feedback

bias detected in our Λ CDM analysis is not detrimental to the joint constraints on w_0 and w_a . It is worth highlighting, however, that the $3 \times 2\text{pt}$ LSST-Y1 analysis will not produce competitive dark energy constraints compared to the combined constraints from existing surveys (see for example figure G2 of DESC-SRD). The most interesting science case for early LSST and *Euclid* data will therefore be the question of tension, both internal tension between different cosmological probes, and external tension with data from the CMB. To ensure confidence in any levels of tension that may be detected, cosmic shear analysis pipelines must become robust to systematic uncertainties within the more constraining Λ CDM framework that we have studied. Developing new observational probes (e.g. Ferreira et al. 2024; McCarthy et al. 2023; Bigwood et al. 2024; Wayland et al. 2025) and flexible theoretical modelling (e.g. Debackere et al. 2020; Mead et al. 2020; Asgari et al. 2023) to constrain baryon feedback will be central to achieving this goal.

We have also reviewed the impact of varying the intrinsic alignment model, finding no significant impact on our constraints. This conclusion comes with a caveat, however, as the response of cosmic shear constraints to changes in the analysis model is known to be dependent on the type of intrinsic alignments that have been simulated in the mock data vector (see for example DK23). In Appendix C we demonstrate that the LSST Y1 S_8 constraints are insensitive to the choice of the cosmological parameter space and Appendix E highlights how adopting a double pass ‘test-truth’ analysis strategy can circumvent the challenges that projection effects introduce when determining a metric of success.

Looking ahead to the conclusion of LSST, we quantify the impact of using a necessarily more complex photometric redshift calibration methodology suited to LSST-Y10. For LSST-Y1, sufficiently deep and representative spectroscopic samples already exist that allow for the use of SOM-based methods to calibrate Y1 photometric redshifts. Moving to the unprecedented wide-field depths of LSST-Y10 however, photometric redshift calibration will have to instead rely on cross-correlation techniques which are currently roughly an order of magnitude less precise than the SOM-based alternative. For our fiducial analysis set-up, we find that this significant degradation in photometric redshift calibration accuracy leaves Y10 no more constraining for S_8 than Y1. Zhang et al. (2026) highlight that the redshift uncertainty on each tomographic bin has a different impact on the constraints and should therefore be treated more carefully than the standard approach we have taken of defining uniform photometric redshift nuisance parameters in forecasts. We leave that extension of our analysis to future work. Nevertheless, this result places a high priority on the development of multi-sample cross-correlation studies which help constrain the changing galaxy bias properties across the full redshift range, enhancing the precision of the resulting photometric redshift calibration (Bernstein 2009). We find that if we can reach a SOM-based accuracy for the Y10 photometric redshifts, and include tight priors on the baryon feedback, Y10 S_8 cosmic shear constraints will be more than five times as constraining as the existing DK23 and DES Collaboration et al. (2026) cosmic shear constraints.

AUTHOR CONTRIBUTIONS

NR: Project Lead for both analysis and paper writing. JZ and CH: Co-wrote paper and assisted with analysis. IM, JS, MS, MD and JS: Developed the FLAMINGO simulations. NS: Assisted with SRD setup and covariance matrix, and provided fisher comparisons. PB: Developed and trained CosmoPower for the analysis. JP: Developed and conducted the different sampler analysis. DL: DESC builder,

contributed to covariance code TJPCov and as internal reviewer.

ACKNOWLEDGEMENTS

This paper has undergone internal review in the LSST Dark Energy Science Collaboration. The internal reviewers were C.D. Leonard, T. Eifler, and R. Mandelbaum.

The DESC acknowledges ongoing support from the Institut National de Physique Nucléaire et de Physique des Particules in France; the Science & Technology Facilities Council in the United Kingdom; and the Department of Energy and the LSST Discovery Alliance in the United States. DESC uses resources of the IN2P3 Computing Center (CC-IN2P3–Lyon/Villeurbanne - France) funded by the Centre National de la Recherche Scientifique; the National Energy Research Scientific Computing Center, a DOE Office of Science User Facility supported by the Office of Science of the U.S. Department of Energy under Contract No. DE-AC02-05CH11231; STFC DiRAC HPC Facilities, funded by UK BEIS National E-infrastructure capital grants; and the UK particle physics grid, supported by the GridPP Collaboration. This work was performed in part under DOE Contract DE-AC02-76SF00515.

We acknowledge the following support: the Max Planck Society and the Alexander von Humboldt Foundation in the framework of the Max Planck-Humboldt Research Award endowed by the Federal Ministry of Education and Research (CH); the UK Science and Technology Facilities Council (STFC) under grant ST/V000594/1 (NR, CH, JZ).

IGM and JS are supported by the Science and Technology Facilities Council (grant number ST/Y002733/1) and have received funding from the European Research Council (ERC) under the European Union’s Horizon 2020 research and innovation programme (grant agreement No 769130).

NŠ is supported in part by the OpenUniverse effort, which is funded by NASA under JPL Contract Task 70-711320, ‘Maximizing Science Exploitation of Simulated Cosmological Survey Data Across Surveys.’

For the purpose of open access, the authors have applied a Creative Commons Attribution (CC BY) licence to any Author Accepted Manuscript version arising from this submission.

AFFILIATIONS

¹ Institute of Astronomy, Royal Observatory Edinburgh, University of Edinburgh, Edinburgh EH9 3HJ, United Kingdom

² Ruhr University Bochum, Faculty of Physics and Astronomy, Astronomical Institute, German Centre for Cosmological Lensing, 44780 Bochum, Germany

³ Waterloo Centre for Astrophysics, University of Waterloo, Waterloo, ON N2L 3G1, Canada

⁴ Department of Physics and Astronomy, University of Waterloo, Waterloo, ON N2L 3G1, Canada

⁵ School of Mathematics, Statistics and Physics, Newcastle University, Newcastle upon Tyne, NE1 7RU, United Kingdom

⁶ Astrophysics Research Institute, Liverpool John Moores University, 146 Brownlow Hill, Liverpool L3 5RF, UK

⁷ Center for Cosmology, Department of Physics and Astronomy, University of California—Irvine, Irvine, CA 92697-4575, USA

⁸ Department of Physics, Duke University, Science Dr, Durham, NC 27710, USA

⁹ Lorentz Institute for Theoretical Physics, Leiden University, PO box 9506, 2300 RA Leiden, the Netherlands

¹⁰ Leiden Observatory, Leiden University, PO Box 9513, 2300 RA Leiden, the Netherlands

REFERENCES

- Abbott T. M. C., et al., 2022, *Phys. Rev. D*, 105, 023520
- Aihara H., et al., 2022, *PASJ*, 74, 247
- Alam S., et al., 2017, *MNRAS*, 470, 2617
- Amodeo S., et al., 2021, *Phys. Rev. D*, 103, 063514
- Amon A., Efstathiou G., 2022, *MNRAS*, 516, 5355
- Amon A., et al., 2022, *Phys. Rev. D*, 105, 023514
- Anbajagane D., Pandey S., Chang C., 2024, arXiv e-prints, arXiv:2409.03822
- Anbajagane D., et al., 2025, *The Open Journal of Astrophysics*, 8, 46158
- Aricò G., Angulo R. E., Contreras S., Ondaro-Mallea L., Pellejero-Ibañez M., Zennaro M., 2021, *MNRAS*, 506, 4070
- Asgari M., et al., 2021, *A&A*, 645, A104
- Asgari M., Mead A. J., Heymans C., 2023, *The Open Journal of Astrophysics*, 6, 39
- Bechtol K., et al., 2025, arXiv e-prints, arXiv:2501.05739
- Berger J. O., Bernardo J. M., Sun D., 2009, *The Annals of Statistics*, 37, 905
- Bernstein G. M., 2009, *ApJ*, 695, 652
- Bernstein G., et al., 2025, arXiv e-prints, arXiv:2506.00758
- Bigwood L., et al., 2024, *MNRAS*, 534, 655
- Bigwood L., et al., 2025a, arXiv e-prints, arXiv:2512.04209
- Bigwood L., Bourne M. A., Iršič V., Amon A., Sijacki D., 2025b, *MNRAS*, 542, 3206
- Blake C., et al., 2025, *The Open Journal of Astrophysics*, 8, 24
- Blazek J. A., MacCrann N., Troxel M. A., Fang X., 2019, *Phys. Rev. D*, 100, 103506
- Bolliet B., Comis B., Komatsu E., Macías-Pérez J. F., 2018, *MNRAS*, 477, 4957
- Boruah S. S., et al., 2024, arXiv e-prints, arXiv:2403.11797
- Bridle S., King L., 2007, *New Journal of Physics*, 9, 444
- Brout D., et al., 2022, *ApJ*, 938, 110
- Buchner J., 2023, *Statistics Surveys*, 17, 169
- Buchs R., et al., 2019, *MNRAS*, 489, 820
- Chang C., et al., 2019, *MNRAS*, 482, 3696
- Chen Z., Yu Y., Han J., Jing Y., 2025, *Science China Physics, Mechanics, and Astronomy*, 68, 289512
- Chintalapati P. R. V., Gutierrez G., Wang M. H. L. S., 2022, *Phys. Rev. D*, 105, 043515
- Chisari N. E., 2025, *A&A Rev.*, 33, 5
- Cordero J. P., et al., 2022, *MNRAS*, 511, 2170
- DES Collaboration et al., 2026, arXiv e-prints, arXiv:2601.14559
- Dalal R., et al., 2023, *Phys. Rev. D*, 108, 123519
- Dalal N., To C.-H., Hirata C., Hyeon-Shin T., Hilton M., Pandey S., Bond J. R., 2025, arXiv e-prints, arXiv:2507.04476
- Dark Energy Survey and Kilo-Degree Survey Collaboration et al., 2023, *The Open Journal of Astrophysics*, 6, 36
- DeRose J., et al., 2022, *Phys. Rev. D*, 105, 123520
- DeRose J., et al., 2023, *J. Cosmology Astropart. Phys.*, 2023, 054
- Debackere S. N. B., Schaye J., Hoekstra H., 2020, *MNRAS*, 492, 2285
- Di Valentino E., et al., 2021, *Astroparticle Physics*, 131, 102604
- Elbers W., et al., 2025, *MNRAS*, 537, 2160
- Euclid Collaboration: Knabenhans M., et al., 2021, *MNRAS*, 505, 2840
- Euclid Collaboration et al., 2025a, arXiv e-prints, arXiv:2510.10021
- Euclid Collaboration et al., 2025b, *A&A*, 697, A1
- Feroz F., Hobson M. P., Bridges M., 2009, *Monthly Notices of the Royal Astronomical Society*, 398, 1601
- Ferreira T., Alonso D., Garcia-Garcia C., Chisari N. E., 2024, *Phys. Rev. Lett.*, 133, 051001
- Fischbacher S., Kacprzak T., Blazek J., Refregier A., 2023, *J. Cosmology Astropart. Phys.*, 2023, 033
- Fortuna M. C., Hoekstra H., Joachimi B., Johnston H., Chisari N. E., Georgiou C., Mahony C., 2021, *MNRAS*, 501, 2983
- Gatti M., et al., 2022, *MNRAS*, 510, 1223
- Georgiou C., et al., 2019, *A&A*, 628, A31
- Graham M. L., Connolly A. J., Ivezić Ž., Schmidt S. J., Jones R. L., Jurić M., Daniel S. F., Yoachim P., 2018, *AJ*, 155, 1
- Gu S., van Waerbeke L., Bernardeau F., Dalal R., 2025, *Phys. Rev. D*, 111, 083530
- Hadzhiyska B., Ferraro S., Farren G. S., Sailer N., Zhou R., 2025, *Phys. Rev. D*, 112, 123507
- Handley W. J., Hobson M. P., Lasenby A. N., 2015, *MNRAS*, 450, L61
- Hastings W. K., 1970, *Biometrika*, 57, 97
- Heavens A. F., Sellentin E., 2018, *J. Cosmology Astropart. Phys.*, 2018, 047
- Heitmann K., Lawrence E., Kwan J., Habib S., Higdon D., 2014, *ApJ*, 780, 111
- Heymans C., et al., 2021, *A&A*, 646, A140
- Hildebrandt H., et al., 2021, *A&A*, 647, A124

- Howlett C., Lewis A., Hall A., Challinor A., 2012, *J. Cosmology Astropart. Phys.*, 2012, 027
- Huang H.-J., Eifler T., Mandelbaum R., Dodelson S., 2019, *MNRAS*, 488, 1652
- Huterer D., 2023, *A&A Rev.*, 31, 2
- Joachimi B., Mandelbaum R., Abdalla F. B., Bridle S. L., 2011, *A&A*, 527, A26
- Joachimi B., et al., 2021, *A&A*, 646, A129
- Johnston H., et al., 2021, *A&A*, 646, A147
- Johnston H., et al., 2025, *A&A*, 699, A127
- Kammerer L., Bartlett D. J., Kronberger G., Desmond H., Ferreira P. G., 2025, *A&A*, 701, A284
- Kilbinger M., et al., 2017, *MNRAS*, 472, 2126
- Krause E., et al., 2021, *arXiv e-prints*, arXiv:2105.13548
- Kugel R., et al., 2023, *MNRAS*, 526, 6103
- La Posta A., Alonso D., Chisari N. E., Ferreira T., García-García C., 2025, *Phys. Rev. D*, 112, 043525
- Lange J. U., 2023, *MNRAS*, 525, 3181
- Laureijs R., et al., 2011, *arXiv e-prints*, arXiv:1110.3193
- Lemos P., et al., 2023, *MNRAS*, 521, 1184
- Leonard C. D., Rau M. M., Mandelbaum R., 2024, *Phys. Rev. D*, 109, 083528
- Lewis A., Challinor A., Lasenby A., 2000, *ApJ*, 538, 473
- Li S.-S., et al., 2023, *A&A*, 679, A133
- Lin S., Li Y., Genel S., Villaescusa-Navarro F., Dai B., Luo W., Wang Y., 2025, *arXiv e-prints*, arXiv:2509.01881
- Lochner M., et al., 2022, *ApJS*, 259, 58
- Mandelbaum R., 2018, *ARA&A*, 56, 393
- Mandelbaum R., Hirata C. M., Ishak M., Seljak U., Brinkmann J., 2006, *MNRAS*, 367, 611
- Martin-Alvarez S., Iršič V., Koudmani S., Bourne M. A., Bigwood L., Sijacki D., 2025, *MNRAS*, 539, 1738
- Martinelli M., et al., 2021, *A&A*, 649, A100
- McCarthy I. G., Schaye J., Bird S., Le Brun A. M. C., 2017, *MNRAS*, 465, 2936
- McCarthy I. G., et al., 2023, *MNRAS*, 526, 5494
- McCarthy I. G., et al., 2025, *MNRAS*, 540, 143
- McCullough J., et al., 2024, *MNRAS*, 531, 2582
- Mead A. J., Peacock J. A., Heymans C., Joudaki S., Heavens A. F., 2015, *MNRAS*, 454, 1958
- Mead A. J., Tröster T., Heymans C., Van Waerbeke L., McCarthy I. G., 2020, *A&A*, 641, A130
- Mead A. J., Brieden S., Tröster T., Heymans C., 2021, *MNRAS*, 502, 1401
- Metropolis N., Rosenbluth A. W., Rosenbluth M. N., Teller A. H., Teller E., 1953, *The Journal of Chemical Physics*, 21, 1087
- Mill C. M., Danielle L. C., Rau M. M., Uhlemann C., Joudaki S., 2025, *J. Cosmology Astropart. Phys.*, 2025, 037
- Mossa V., et al., 2020, *Nature*, 587, 210
- Myles J., et al., 2023, *MNRAS*, 519, 1792
- Neal R. M., 2003, *The Annals of Statistics*, 31, 705
- Newman J. A., 2008, *ApJ*, 684, 88
- Newman J. A., Gruen D., 2022, *ARA&A*, 60, 363
- Pakmor R., et al., 2023, *MNRAS*, 524, 2539
- Pandey S., et al., 2023, *MNRAS*, 525, 1779
- Piccirilli G., Zennaro M., García-García C., Alonso D., 2025, *J. Cosmology Astropart. Phys.*, 2025, 017
- Planck Collaboration 2020, *A&A*, 641, A6
- Porredon A., et al., 2025, *arXiv e-prints*, arXiv:2512.15960
- Prat J., et al., 2023, *The Open Journal of Astrophysics*, 6, 13
- Preston C., Amon A., Efstathiou G., 2023, *MNRAS*, 525, 5554
- Reichardt C. L., et al., 2021, *ApJ*, 908, 199
- Reischke R., 2024, *MNRAS*, 530, 4412
- Reischke R., Hagstotz S., 2025, *arXiv e-prints*, arXiv:2507.17742
- Riess A. G., et al., 2018, *ApJ*, 861, 126
- Riess A. G., et al., 2022, *ApJ*, 938, 36
- Robertson N. C., Hall A., 2025, *arXiv e-prints*, arXiv:2512.15604
- Ruiz-Zapatero J., Hadzhiyska B., Alonso D., Ferreira P. G., García-García C., Mootoovaloo A., 2023, *MNRAS*, 522, 5037
- Salcido J., McCarthy I. G., Kwan J., Upadhye A., Font A. S., 2023, *MNRAS*, 523, 2247
- Samuroff S., Campos A., Porredon A., Blazek J., 2024, *The Open Journal of Astrophysics*, 7, 40
- Sanchez-Cid D., et al., 2026, *arXiv e-prints*, arXiv:2601.14859
- Schaller M., Schaye J., Kugel R., Broxterman J. C., van Daalen M. P., 2025, *MNRAS*, 539, 1337
- Schaye J., et al., 2010, *MNRAS*, 402, 1536
- Schaye J., et al., 2023, *MNRAS*, 526, 4978
- Schneider A., Teyssier R., 2015, *J. Cosmology Astropart. Phys.*, 2015, 049
- Scolnic D. M., et al., 2018, *ApJ*, 859, 101
- Semboloni E., Hoekstra H., Schaye J., van Daalen M. P., McCarthy I. G., 2011, *MNRAS*, 417, 2020
- Semboloni E., Hoekstra H., Schaye J., 2013, *MNRAS*, 434, 148
- Sheldon E. S., Becker M. R., MacCrann N., Jarvis M., 2020, *ApJ*, 902, 138
- Sheldon E. S., Becker M. R., Jarvis M., Armstrong R., LSST Dark Energy Science Collaboration 2023, *The Open Journal of Astrophysics*, 6, 17
- Siegel J., et al., 2025a, *arXiv e-prints*, arXiv:2507.11530
- Siegel J., et al., 2025b, *arXiv e-prints*, arXiv:2512.02954
- Skilling J., 2006, *Bayesian Analysis*, 1, 833
- Spurio Mancini A., Bose B., 2023, *The Open Journal of Astrophysics*, 6, 40
- Spurio Mancini A., Piras D., Alsing J., Joachimi B., Hobson M. P., 2022, *MNRAS*, 511, 1771
- Stanford S. A., et al., 2021, *ApJS*, 256, 9
- Stölzner B., Joachimi B., Korn A., Hildebrandt H., Wright A. H., 2021, *A&A*, 650, A148
- Sugiyama S., Takada M., Kobayashi Y., Miyatake H., Shirasaki M., Nishimichi T., Park Y., 2020, *Phys. Rev. D*, 102, 083520
- Sunseri J., Amon A., Dunkley J., Battaglia N., Ferraro S., Hadzhiyska B., Ried Guachalla B., Schaen E., 2025, *arXiv e-prints*, arXiv:2505.20413
- Takahashi R., Sato M., Nishimichi T., Taruya A., Oguri M., 2012, *ApJ*, 761, 152
- The LSST Dark Energy Science Collaboration: Mandelbaum R., et al., 2018, *arXiv e-prints*, arXiv:1809.01669
- To C.-H., Pandey S., Krause E., Dalal N., Anbajagane D., Weinberg D. H., 2024, *J. Cosmology Astropart. Phys.*, 2024, 037
- Tröster T., et al., 2020, *A&A*, 633, L10
- Tröster T., et al., 2022, *A&A*, 660, A27
- Truttero O., Zuntz J., Pourtsidou A., Robertson N., 2025, *The Open Journal of Astrophysics*, 8, 19
- Wayland A., Alonso D., Zennaro M., 2025, *MNRAS*, 543, 1518
- White M., 2004, *Astroparticle Physics*, 22, 211
- Wolz L., Kilbinger M., Weller J., Giannantonio T., 2012, *J. Cosmology Astropart. Phys.*, 2012, 009
- Wright A. H., Hildebrandt H., van den Busch J. L., Heymans C., 2020, *A&A*, 637, A100
- Wright A. H., et al., 2024, *A&A*, 686, A170
- Wright A. H., et al., 2025a, *A&A*, 703, A144
- Wright A. H., et al., 2025b, *A&A*, 703, A158
- Yin B., et al., 2025, *arXiv e-prints*, arXiv:2510.23566
- Zanoletti C. M. A., Leonard C. D., 2025, *Phys. Rev. D*, 112, 063547
- Zhang Z., Sheldon E. S., Becker M. R., 2023a, *The Open Journal of Astrophysics*, 6, 16
- Zhang T., Rau M. M., Mandelbaum R., Li X., Moews B., 2023b, *MNRAS*, 518, 709
- Zhang T., et al., 2026, *MNRAS*, 545, staf1829
- Zuntz J., et al., 2015, *Astronomy and Computing*, 12, 45
- d'Assignies W., et al., 2025, *arXiv e-prints*, arXiv:2510.23565
- van Daalen M. P., Schaye J., Booth C. M., Dalla Vecchia C., 2011, *MNRAS*, 415, 3649
- van Daalen M. P., McCarthy I. G., Schaye J., 2020, *MNRAS*, 491, 2424
- van Daalen M. P., Koutalios I., Broxterman J. C., Wolfs B. J. H., Helly J. C., Schaller M., Schaye J., 2026, *MNRAS*, 545, staf2086

lensing window function, q is given by

$$q^i(\chi) = \frac{3H_0^2\Omega_m}{2c^2} p(\ell) \frac{\chi}{a(\chi)} g^i(\chi). \quad (\text{A2})$$

We adopt the extended first-order Limber flat-sky approximation (Kilbinger et al. 2017) where

$$p(\ell) = \frac{\ell^2}{(\ell+1/2)^2}. \quad (\text{A3})$$

APPENDIX

A. COSMIC SHEAR THEORY

The cosmic shear convergence power spectrum, in a spatially flat cosmology, is related to the non-linear matter power spectrum $P_{\text{mm}}(k)$, by

$$C_{\gamma\gamma}^{ij} = \int d\chi \frac{q^i(\chi)q^j(\chi)}{\chi^2} P_{\text{mm}} \left(k = \frac{\ell+1/2}{\chi}, z(\chi) \right), \quad (\text{A1})$$

for tomographic bins i, j , 3D wavenumber k and 2D multipole ℓ . Here χ is the comoving distance and the weak

The lensing kernel for tomographic bin i is given by

$$g^i(\chi) = \int_{\chi}^{\chi_{\text{hor}}} d\chi' n_s^i(\chi') \frac{\chi' - \chi}{\chi'}, \quad (\text{A4})$$

for a source redshift distribution $n_s^i(z) = n_s^i(\chi) d\chi/dz$.

The observed correlation between galaxy shapes includes contributions from both weak lensing by large-scale structure (denoted ‘ γ ’), and the physical intrinsic alignment of neighbouring galaxies (denoted ‘ Γ ’), with the observed cosmic shear power spectrum given by

$$C^{ij}(\ell) = C_{\gamma\gamma}^{ij}(\ell) + C_{\text{II}}^{ij}(\ell) + C_{\gamma\Gamma}^{ij}(\ell), \quad (\text{A5})$$

where

$$C_{\text{ab}}^{ij}(\ell) = \int d\chi \frac{W_a^i(\chi) W_b^j(\chi)}{\chi^2} P_{\text{mm}} \left(k = \frac{\ell + 1/2}{\chi}, z(\chi) \right), \quad (\text{A6})$$

with the shear kernel $W_{\gamma}^i(\chi) = q^i(\chi)$. In this analysis we adopt the redshift-dependent non-linear linear alignment model (NLA- z), where the intrinsic alignment kernel $W_{\Gamma}^i(\chi)$ is given by

$$W_{\Gamma}^i(\chi) = -A_{\text{IA}} \left[\frac{1+z(\chi)}{1+z_0} \right]^{\eta_{\text{IA}}} \frac{\bar{C}_1 \rho_{\text{crit}} \Omega_{\text{m}}}{D(z(\chi))} n_s^i(\chi). \quad (\text{A7})$$

Here $D(z)$ is the linear growth factor, \bar{C}_1 is a normalisation constant and z_0 is the pivot redshift which we fix at $z_0 = 0.62$ (Bridle & King 2007; Joachimi et al. 2011).

We calculate the cosmic shear power spectrum, $C(\ell)$, (Equation A5) with COSMOSIS using the PROJECT2D.PY module. When creating the mock LSST data, the linear matter power spectrum is computed using CAMB (Lewis et al. 2000; Howlett et al. 2012), the gravity-only non-linear correction is estimated using HMCODE2020 in the ‘no feedback’ mode (Mead et al. 2021) and additional suppression from baryon feedback is modelled using data from the Schaye et al. (2023) FLAMINGO hydrodynamical simulation (see Section 2.2.1 for details).

When analysing the mock cosmic shear data we use the COSMOPOWER neural network suite to emulate the non-linear matter power spectrum, $P_{\text{mm}}(k, z)$, including baryon feedback (Spurio Mancini et al. 2022). We train COSMOPOWER within our chosen multi-dimensional parameter space (see Table 2) using 450,000 power spectra calculated with CAMB and HMCODE2020, now in feedback mode. For our fiducial Y1 cosmic shear analysis in Section 3.1, we verify that our parameter constraints using COSMOPOWER are within 0.1σ from an analysis that uses CAMB +HM-CODE2020 directly, finding the runtime when using COSMOPOWER is a factor of four faster. We note that for the analyses which extend the parameter space, for example varying neutrino mass in Section C.3 and constraining dark energy parameters in Section 3.5, we revert back to the full CAMB and HMCODE2020-based analysis, rather than re-training the emulator.

B. MOCK LSST OBSERVATIONS

Our mock LSST cosmic shear observations adopt DESC-SRD defined parameters for the Y1 and Y10 survey area, depth, shear and redshift precision, as listed with explicit references for each value in Table 1. We note that a series of survey cadence optimisation studies have recommended a revision to the DESC-SRD-adopted LSST design, increasing the survey area by $\sim 25\%$ with little degradation in depth as a result of improvements in the anticipated system throughput¹³. As our forecasts show that without improve-

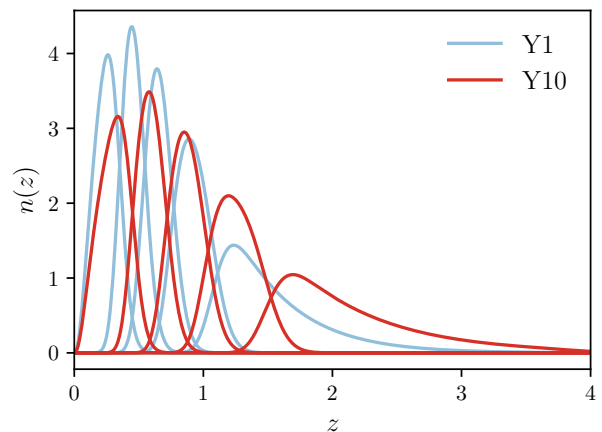


Figure 9. Tomographic redshift distributions used in mock spectrum calculation for our Y1 and Y10. An outlier population is included by spreading 7% of the sample uniformly in the range $0 < z < 3$. The mean redshift of Y1 is $\langle z \rangle = 0.85$ and for Y10 is $\langle z \rangle = 1.05$.

ments to our understanding of baryon feedback and redshift calibration, LSST cosmic shear constraints will be systematics dominated, this expected increase in survey area will not alter our conclusions.

We determine the redshift bins by taking the DESC-SRD parameterised redshift distribution for the full Y1 and Y10 samples, split into five equally populated slices and convolved with a Gaussian error distribution of width $\sigma_i = 0.05(1 + \bar{z}_i)$. Here \bar{z}_i is the mean redshift of the i ’th bin. This approach to developing a redshift bin model does not include ‘catastrophic outliers’, unfortunately resulting in an unrealistically low level of overlap between non-adjacent bins. For cosmic shear forecasts interested in optimising scale cuts, the use of idealistic clean and narrow photometric redshift bins could be problematic as they allow for scale cuts in the 2D ℓ -projection to be more closely related to the desired physical scale cut in k .

LSST catalogue simulations from Graham et al. (2018) derive a photometric redshift outlier population using a colour-space nearest-neighbour technique, finding the majority of outliers lie at either very high ($z > 2$) or very low ($z < 0.5$) redshifts. Assuming the shape of this outlier redshift distribution is known, Boruah et al. (2024) find that the outlier fraction must be accurate to within 5-10% in order to achieve unbiased cosmological parameter constraints. In this analysis we do not revisit the question of uncertainty in the outlier fraction. Instead, assuming that the shape of the full redshift distribution, including outliers, is known accurately for each bin, we marginalise over our uncertainty on the mean redshift of each tomographic distribution. We do, however, choose to enhance the realism of the DESC-SRD redshift distribution model by including outliers, adopting a ‘worse case scenario’ for mixing k -scales by distributing a 7% outlier fraction uniformly across the full redshift range from $0 < z < 3$. This model, shown in Figure 9, is motivated by a self-organising map (SOM) analysis of photometric redshifts in the COSMOS field, which results in a 7% outlier fraction population fairly equally distributed across the full redshift range (Stanford et al. 2021). We note that the different outlier population distributions in Graham et al. (2018) and Stanford et al. (2021) could result from their contrasting approaches to photometric redshift estimation.

We calculate the forecast covariance on the LSST cosmic shear power spectrum using TJPcov¹⁴. We refer the reader to section 5.2 and appendix E.1 of Joachimi et al. (2021) for a discussion of the various terms that contribute

¹³ The LSST Survey Cadence Optimisation Committee’s Phase 2 Recommendations are published in the internal LSST document PSTN-055.

¹⁴ The DESC Theory Joint Probe Covariance open source code, TJP-COV, is available at github.com/LSSTDESC/tjpcov.

to the covariance. In this analysis we include the Gaussian terms which account for shot-noise from the galaxy shear measurements (with $\sigma_e = 0.26$), finite area sampling variance, and the mix between these two error terms. We also use the TJPCOV analytic halo model to calculate the super-sample covariance which encodes the impact of Fourier modes larger than the survey window. We do not include the non-Gaussian terms, as these are fairly insignificant for cosmic shear. Instead the final term we include accounts for the statistical uncertainty in the shear calibration correction, where $\sigma_{m,i} = 0.002(1 + \bar{z}_i)$ (as discussed in Section 2.1), assuming 100% correlation between the redshift bins (see equation 37 of Joachimi et al. 2021).

C. COSMOLOGICAL PARAMETERS AND PRIORS

In every cosmological analysis, there is a choice to be made on the set of cosmological parameters and corresponding priors. With no standardised method to determine these choices, some surveys choose a parameter space optimised for the observable (see for example the discussion in Tröster et al. 2020), with others choosing a Λ CDM space with different forms for the density parameters (for example Ω_m or $\omega_c = [\Omega_m - \Omega_b] h^2$), the power spectrum amplitude parameters (A_s , σ_8 or S_8), and the dark energy extension. Priors can be chosen to be informative based on constraints from complementary analyses. Alternatively uninformative priors can be selected, although it is challenging to ensure that the complete prior set is truly uninformative¹⁵. In cases of unconstrained parameters with weakly informative priors that are asymmetric around the truth, Chintalapati et al. (2022) and DK23 demonstrate projection effects within the marginal posterior distributions of constrained parameters, quantifying tension between 1D-marginal statistics and the underlying true cosmology. The definition of the cosmological set of parameters and priors, therefore matters, when comparing constraints from different surveys.

In Table 2 we list our parameter set and priors, comparing our choices to DESC-SRD which are more informative in all but the notable case of the dark energy parameters. We adopt uninformative priors for the cosmic shear-constrained parameters: $\Omega_m, \sigma_8, A_{IA}, \eta_{IA}$. All other parameters have informative priors, as shown in Figure 10 where we compare the multi-dimensional prior volume with the posterior from the fiducial analysis presented in Section 3.1.

To set the limits of our uninformative priors we adopt tophat priors, using literature-defined $\pm 7\sigma$ regions for the breadth. For Ω_m , we take constraints from the *Pantheon+* analysis of supernova type Ia (Brout et al. 2022), defining a tophat prior with $\pm 7\sigma$ *Pantheon*-informed edges of $\Omega_m \in [0.2, 0.46]$. For σ_8 , we adopt a $\pm 7\sigma$ region defined by the 3×2 pt analysis of DES Y3 (Abbott et al. 2022) with $\sigma_8 \in [0.39, 1.01]$. Note that a $\pm 7\sigma$ region defined by Planck Collaboration (2020), in either parameter, would be informative in our analysis.

Setting informative priors requires some subjectivity. For ω_b the choice is relatively clear, with two independent observables reporting similar results: $\omega_b^{\text{CMB}} = 0.02237 \pm 0.00015$ (Planck Collaboration 2020) and $\omega_b^{\text{BBN}} = 0.02233 \pm 0.00036$ (Mossa et al. 2020). We take the more conservative of the two using a Gaussian prior $\omega_b \in \mathcal{N}(0.02233, 0.00036)$, sampling in ω_b rather than Ω_b to en-

¹⁵ Consider two cases where a flat prior has been adopted for Ω_m and ω_c respectively. Even if the resulting posteriors are insensitive to the breath of these priors, the different dependencies of the priors on h and Ω_b will influence the posterior's shape. The standard statistical approach of determining the uninformative Jeffreys prior does not apply in a multi-dimensional space. Reference priors (Berger et al. 2009; Heavens & Sellentin 2018) provide a multi-dimensional alternative to Jeffreys, but these have yet to be explored in detail by the cosmological community.

sure that this externally constrained prior remains separate from our uncertainty over the value of h where there are a number of disparate constraints. Constraints from the CMB favour low values of H_0 with $H_0^{\text{CMB}} = 67.36 \pm 0.54$ (Planck Collaboration 2020). Direct measurements from Cepheid observations favour higher values with $H_0^{\text{SHOES}} = 73.15 \pm 0.97$ (Riess et al. 2022). We choose to use a tophat prior with the lower edge defined as -5σ from the *Planck* best-fit, and the upper edge defined as $+5\sigma$ from the SHOES constraint, $h : [0.65, 0.78]$. For n_s we motivate the width of the prior set using the $\pm 5\sigma$ region of the n_s constraint from Planck Collaboration (2020). We also include additional prior knowledge here by centering our prior around the theoretical expectation for n_s such that $n_s : [0.95, 0.99]$.

C.1. Sensitivity to the parameter set: σ_8 or A_s

Cosmic shear constraints from existing surveys have been shown to be sensitive to the choice of the power spectrum amplitude parameter within the sampling set (see for example Chang et al. 2019). Traditionally cosmic shear surveys sampled using flat priors for either A_s or $\ln A_s$, but this approach is no-longer favoured¹⁶, given the non-trivial way a nominally uninformative prior on A_s or $\ln A_s$, informs both Ω_m and σ_8 (Joachimi et al. 2021). The alternative approach of sampling in $S_8 = \sigma_8(\Omega_m/0.3)^\alpha$, where $\alpha = 0.5$, ensures uninformative priors on this composite parameter, but given the uncertainty on the optimal α -value for higher-redshift Stage-IV surveys (Wright et al. 2025b), we have chosen to sample over σ_8 for our fiducial analysis. Interestingly, we found that this choice was rather a moot point: in a robustness test of our fiducial analysis, where we sampled over A_s , we found less than 0.1σ differences between our constrained parameters with the associated uncertainty differing by less than a few percent. Within the statistical power on LSST, we can therefore conclude that the cosmic shear constraints are insensitive to the parameter chosen to model variations in the power spectrum amplitude.

C.2. Sensitivity to the informative prior width: h_0 and n_s

In Figure 11 we compare our fiducial analysis from Section 3.1 with an alternative analysis that adopts the cosmological parameter priors from Amon et al. (2022). Their priors on the unconstrained set of parameters are significantly wider than our fiducial set-up in Table 2, with $h_0 \in [0.55, 0.91]$, $n_s \in [0.87, 1.07]$, and $\Omega_b \in [0.03, 0.07]$. Despite increasing the prior width, these priors nevertheless remain informative, as these particular parameters cannot be constrained by cosmic shear alone. We find the S_8 constraining power reduced by $\sim 4\%$ when adopting this weaker set of priors, resulting from weak degeneracies in $h_0 - \Omega_m$ and $n_s - S_8$. In principle the informative priors on these parameters could be extended further, continuing to expand the allowed constrained region in the projected $S_8 - \Omega_m$ plane. But as these regions in the multi-dimensional parameter space can be easily ruled out from other data sets, our preference is to use the tighter informed priors listed in Table 2.

It is worth noting the strong degeneracy between h_0 and n_s in Figure 11. This feature inadvertently leads to an artificial constraint on n_s being reported in the LSST-Y1 cosmic shear forecast of Prat et al. (2023). In that case, a strongly

¹⁶ We note that Sugiyama et al. (2020) derive a correction weight to convert a chain that has been efficiently sampled using uninformative flat priors in (Ω_m, A_s) , in order to achieve the desired uninformative priors in (Ω_m, σ_8) in the cosmic shear analysis of HSC (Dalal et al. 2023). We experimented using this approach but chose not to adopt it. As the proposed weighting scheme is only correct to first-order, we found that it lead to a significant slope in the effective Ω_m -prior without significantly resolving the issue of the artificial truncation of the $\Omega_m - \sigma_8$ degeneracy highlighted by Joachimi et al. (2021).

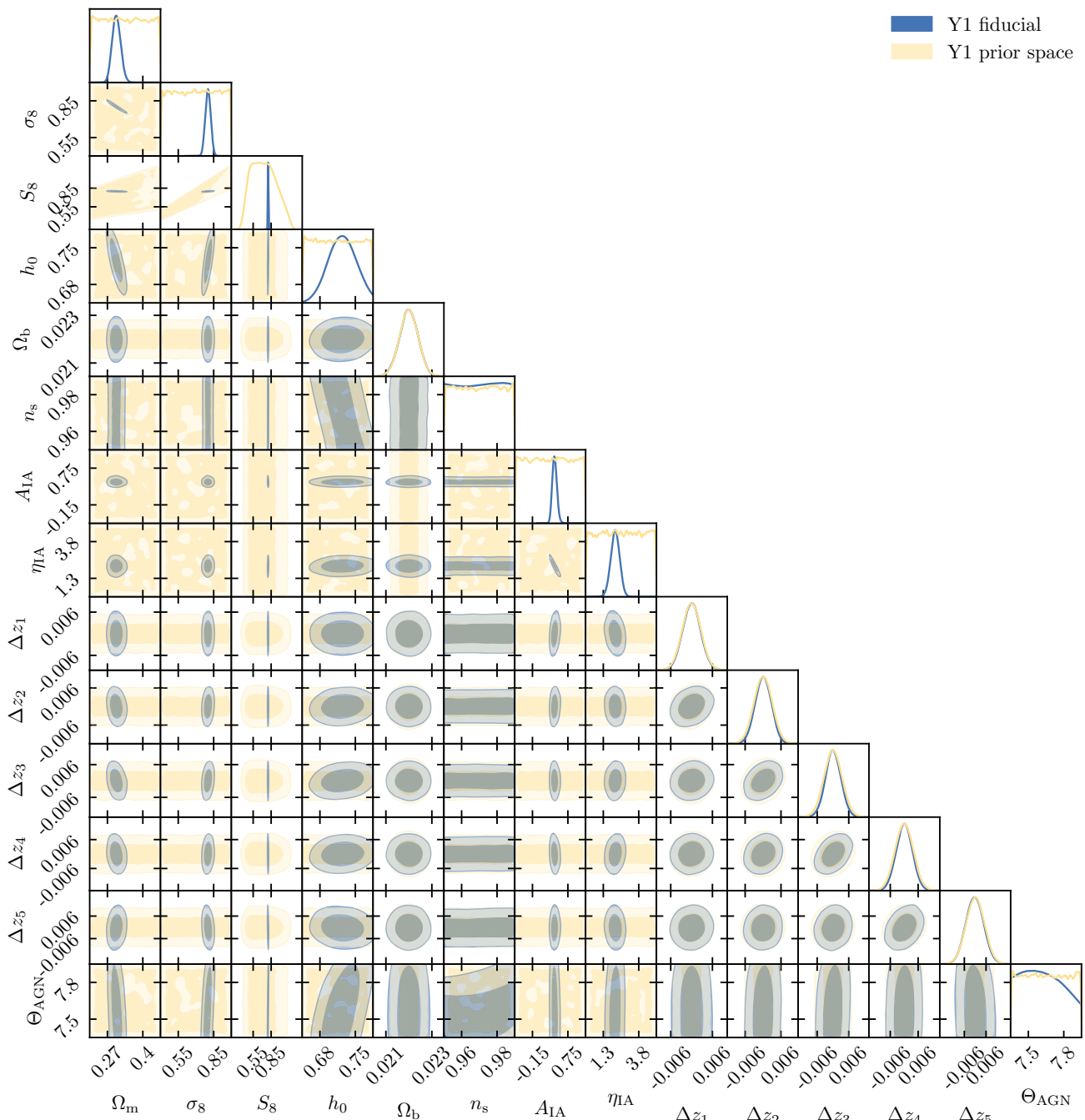


Figure 10. Comparison of samples from the prior (green) and posterior constraints (blue), under our fiducial analysis. Only Ω_m , σ_8 , S_8 , A_{IA} and η_{IA} are likelihood-dominated; the others are prior-dominated. The choice of priors on the other parameters is important, however; as shown in Figure 11: some choices can lead to apparent constraints not driven by data.

informative prior placed on h_0 introduced what appeared to be a data constraint on the weakly informed n_s parameter. With a different set of priors, the converse could also have occurred making it appear that h_0 was data-constrained. We caution that degeneracies between all parameters should be carefully reviewed within the prior volume (see Figure 10) before concluding that constraints are data-driven.

C.3. Varying the sum of neutrino masses

Cosmic shear analyses are fairly insensitive to variations in the sum of neutrino masses, especially when applying scale cuts and/or marginalising over a range of baryon feedback scenarios (Spurio Mancini & Bose 2023). In our fiducial analysis we therefore adopt the theoretically preferred value for $\Sigma m_\nu = 0.006\text{eV}$, testing the robustness of this decision with a test analysis where we adopt a top hat prior of $\Sigma m_\nu \in [0.05, 0.6]\text{eV}$ following Amon et al. (2022). As ex-

pected, Σm_ν is unconstrained by our analysis, and the inclusion of this additional parameter has no significant impact on the precision of S_8 or Ω_m measurements. We draw the same conclusions as DK23, however, that the introduction of a free Σm_ν parameter significantly shifts the position of the mean and maximum of the marginal S_8 distribution as a result of projection effects (see the discussion in section 3.2 of DK23). Our ‘truth’ analysis quantifies the projection ‘bias’ in this case, finding that it shifts the mean marginal to $\sim 0.8\sigma$ below the input cosmological value.

D. SAMPLER CHOICE

In this section, we compare different sampling algorithms available through COSMOSIS¹⁷ for characterising our fiducial LSST Y1 model posteriors. There are many

¹⁷ COSMOSIS: github.com/cosmosis-developers/cosmosis

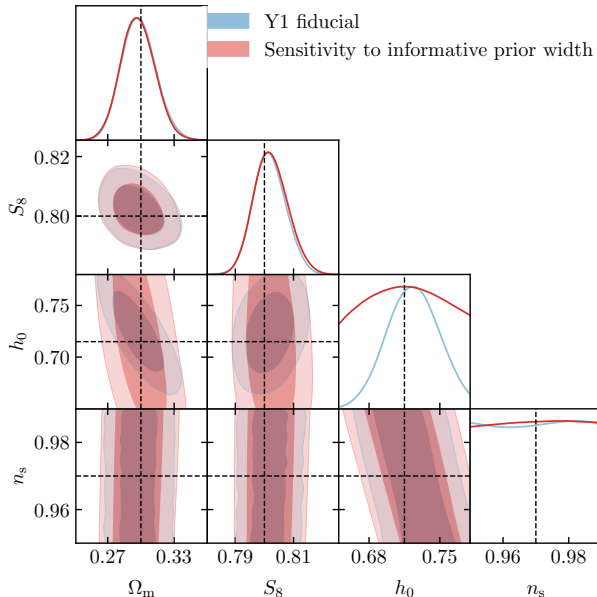


Figure 11. Constraints comparing the Y1 fiducial analysis (blue) to an analysis with less informative priors on the unconstrained parameters Ω_b , h_0 , and n_s (red). We find a 4% increase in the uncertainty on S_8 under the broader priors. The $h_0 - n_s$ constraints highlight the degeneracy between these two parameters in cosmic shear, such that a strongly informative prior on n_s will result in h_0 apparently being constrained, and vice versa.

different ways to sample from a probability distribution; most cosmological analyses have used either *Markov Chain Monte Carlo* (MCMC) methods, especially the Metropolis-Hastings (Metropolis et al. 1953; Hastings 1970) and *nested sampling* (Skilling 2006) algorithms. Like many recent cosmic shear studies, we focus here on nested sampling methods since they generally require less tuning for specific problems, and also provide the Bayesian Evidence quantity that can be used for model comparisons.

Nested sampling (NS) is designed for exploring complex, multi-modal likelihoods and for model comparison. Generically, it integrates from the bounds of a prior distribution in towards the peaks(s) of the posterior, using an ensemble of *live points* in the parameter space. By successively replacing the lowest likelihood point and replacing it with a new point, it attempts to evenly sample the subspace of increasingly higher likelihood.

There are many different NS algorithms and software packages; see Buchner (2023) for a recent review. Here we compare the behaviour of three NS algorithms for our use case: MULTINEST¹⁸, POLYCHORD¹⁹, and NAUTILUS²⁰. In each case we use the CosmoSIS default parameters for these samplers²¹ except as specified below.

MULTINEST is an NS algorithm originally designed for multi-modal distributions and curving degeneracies in high dimensions (Feroz et al. 2009). It builds ellipsoids around the set of live points and samples within them. However, as the number of dimensions of a problem increases its number of likelihood evaluations increases exponentially (Handley et al. 2015). Here we use MULTINEST with 675 live points and efficiency 1.0.

POLYCHORD uses *slice sampling* (Neal 2003), generating points within 1D slices of constant posterior in the multi-dimensional parameter space (Handley et al. 2015). It can take a long time to complete but generally scales well with dimensionality. Here we use POLYCHORD with 250 live points and 30 repeats.

¹⁸ MULTINEST: github.com/farhanferoz/MultiNest

¹⁹ POLYCHORD: github.com/PolyChord/PolyChordLite

²⁰ NAUTILUS: github.com/johannesul/nautilus

²¹ <https://cosmosis.readthedocs.io/en/latest/usage/samplers.html>

NAUTILUS uses deep learning to build a model of where to propose new live points, based on all previously sampled points (Lange 2023). This algorithm runs in parallel, which is beneficial for large data sets. We use NAUTILUS with 2000 live points, 512 batches, and 16 networks.

We ran each algorithm on our fiducial model on two 128-core nodes on the National Energy Research Scientific Computing Center (NERSC) machine *Perlmutter*, with 64 processes and four threads per process. We ran our fiducial analysis configuration (which uses COSMOPower) as described in Sec. 3.1. In this configuration, MULTINEST completed in 0.83 hours, POLYCHORD in 6.2 hours, and NAUTILUS in 0.86 hours. We use the default stopping criteria for each sampler, which are all slightly different, so potentially any could have attained similar results faster with careful tuning, but the large difference between POLYCHORD and the other two would almost certainly remain. Contours in the primary $\Omega_m - \sigma_8$ space for the three models agreed very well; 68% and 95% chain quantiles of selected marginalised parameter values for the three methods are shown in Figure 12.

All samplers can have different levels of success when applied to new posteriors, requiring tests to be performed on sampling methods when beginning any large analysis campaigns. Late Stage III 3×2 pt posteriors, for example, have proven particularly problematic for recent sampling methods (Sanchez-Cid et al. 2026). For our analysis, all three samplers recover the same constraints. We choose not to use the slightly faster MULTINEST sampler, as this has been shown in other studies to underestimate the size of the credible intervals in less constraining cosmic shear studies (see appendix D of DK23 and Lemos et al. 2023). Given its speed advantage over POLYCHORD, and the tests against other samplers reported in Lange (2023), we adopt NAUTILUS for this project.

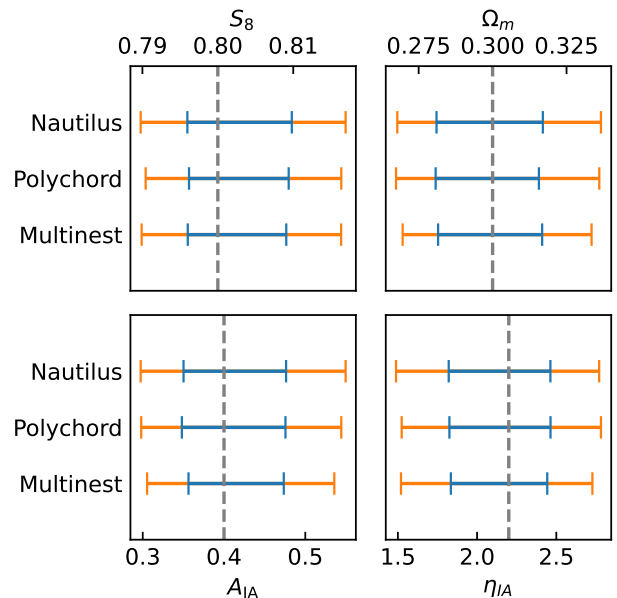


Figure 12. 68% and 95% quantiles of selected parameters under our fiducial model compared using the POLYCHORD, MULTINEST, and NAUTILUS sampling algorithms. In our scenario the three methods perform equally well, producing near-identical contours for all parameters of interest. We adopt NAUTILUS for the other chains in this work because of its speed and robustness.

E. MITIGATING PROJECTION BIAS

We optimise our analysis choices based on the accurate recovery of S_8 , as determined by the difference be-

| Feedback strength | | Weak | Fiducial | Strong |
|-------------------|--------------------------|--------------------------|----------|---------------------|
| FLAMINGO ID | | $f_{\text{gas}+2\sigma}$ | L1_m9 | Jet_fgas-4 σ |
| HMCODE2020: | Θ_{AGN} | 7.562 | 7.694 | 7.931 |
| SP(κ): | ϵ | 0.350 | 0.316 | 0.251 |
| | α | 0.340 | 0.100 | -0.120 |
| | β | 0.770 | 0.817 | 0.740 |
| | γ | 1.190 | 0.800 | 1.020 |
| | $\log(m_{\text{pivot}})$ | 13 | 13 | 13 |

Table 5. The baryon feedback parameters used to create ‘truth’ mocks for the three ‘test’ FLAMINGO models.

tween the projected mean marginal constraint on S_8 from a ‘truth’ and ‘test’ analysis. In Table 5 we list the HMCODE2020 and SP(κ) baryon feedback parameters used to create ‘truth’ mocks for the three ‘test’ FLAMINGO models. These parameters were found to provide the best-fits to the FLAMINGO-created LSST-Y1 cosmic shear power spectra, when analysing all scales with all other parameters fixed to the input values listed in Table 2.

In the development of this work we also explored the alternative approach of using the MAP (maximum a posteriori) to define success. In the case of a ‘truth’ analysis, a noise-free MAP estimate will return the input cosmological parameters, arguably making this summary statistic optimal for the assessment of parameter bias without any complications arising from projection bias. To obtain the MAP, we used the MAXLIKE sampler within COSMOSIS which performs an optimisation process to find the peak of the likelihood. With the results of a NAUTILUS MCMC analysis to define the starting position, we ran the MAXLIKE sampler 20 times. The set of parameters corresponding to the maximum posterior value from those 20 estimates can then be defined as the MAP.

In an analysis of numerous suites of 20 noisy MAP S_8 estimates, we noted significant $\sim 0.5\sigma$ differences, even though there was negligible change in the posterior value. We concluded that as cosmic shear only constrains S_8 and Ω_m , the MAXLIKE sampler’s exploration of the wide regions of unconstrained parameter space leads to real variations between the estimated S_8 location of the MAP. As our metric of success is tied to the accurate recovery of the single most-constrained parameter, and not the accurate recovery of all parameters, we concluded that the MAP was therefore not the most appropriate statistic to use for our study.

F. ADDITIONAL DATA TABLES AND FIGURES

F.1. Modelling intrinsic alignments with TATT

Figure 13 shows constraints when analysing our fiducial mock, which includes NLA-z intrinsic alignments, with the extended TATT IA model. TATT is a super-set of NLA-z, which adds a tidal torquing alignment mechanism with new amplitude, $A_{\text{IA},2}$, redshift scaling $\eta_{\text{IA},2}$ and a linear galaxy bias amplitude, bias_{ta} parameters for the new component. Our TATT parameter priors follow Abbott et al. (2022), which are uninformative for LSST-Y1, except in the case²² of $\eta_{\text{IA},2}$. In Figure 13 we can see that the use of the more flexible model has no effect on S_8 constraints; the same is also true of the other primary cosmological parameters. This does not indicate that TATT should be used in place of NLA in all analyses; while it is a more physically motivated

²² For cases where the true value of either intrinsic alignment amplitude $A_{\text{IA},i} = 0$, it becomes challenging to set a lower limit on the corresponding redshift scaling parameter $\eta_{\text{IA},i}$. For a low value of $A_{\text{IA},i}$, a large negative value for $\eta_{\text{IA},i}$ can remain acceptable as it only serves to alter the strength of the intrinsic alignment model at very low redshift where the signal-to-noise of the data is insufficient to rule out the model. For this reason the lower bound of the posterior for the TATT parameter $\eta_{\text{IA},2}$ will not close in an NLA-z mock analysis, even with an extended prior.

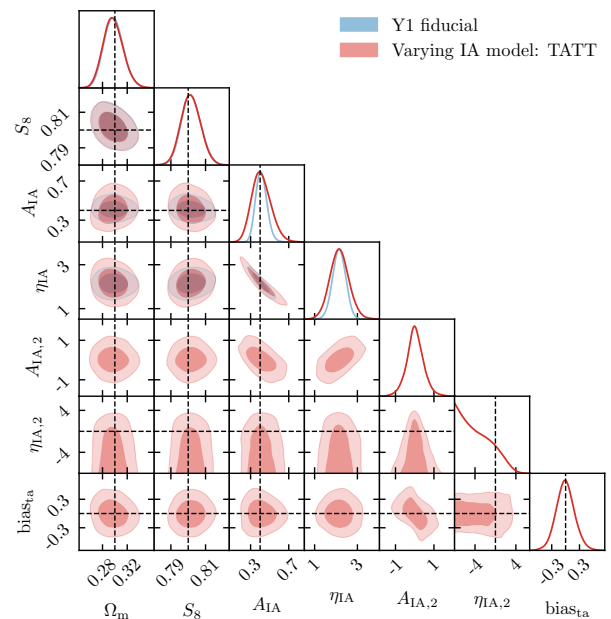


Figure 13. Constraints on our primary parameters under our fiducial NLA-z IA analysis (blue) versus an extended TATT analysis, both of an NLA-z mock. Switching to the broader TATT model has no effect on the S_8 precision or accuracy. The more flexible TATT model can, however, absorb any errors in photometric redshift modelling, leading to cosmological biases.

model that can capture more general galaxy alignment behaviour, Samuroff et al. (2024) have shown that this can lead to parameter biases in the presence of photometric redshift uncertainty.

F.2. Data tables

We express our scale cut choices as cuts in wave-number k , which we then translate to per-bin angular scale cuts using the corresponding distance in our truth model to the median redshift of each tomographic bin (see Equation 1). Table 3 lists the ℓ cuts for each K_{max} cut that we consider. Tables 8 collects measurements of precision and accuracy metrics for different baryon feedback simulations in the Y1 mock and two different methods for modelling, HMCODE2020 and SP(κ).

This paper was built using the Open Journal of Astrophysics \LaTeX template. The OJA is a journal which provides peer review for new papers in the `astro-ph` section of the arXiv. Learn more at <http://astro.theoj.org>.

| z -bin | $\langle z \rangle$ | ℓ_{\max} | | | | | |
|----------------|---------------------|------------------|------------------|------------------|------------------|------------------|----------------|
| | | $K_{\max} = 0.1$ | $K_{\max} = 0.2$ | $K_{\max} = 0.4$ | $K_{\max} = 0.5$ | $K_{\max} = 0.6$ | $K_{\max} = 1$ |
| 1 | 0.26 | 83 | 165 | 331 | 413 | 496 | 827 |
| 2 | 0.46 | 120 | 240 | 480 | 600 | 720 | 1200 |
| 3 | 0.66 | 143 | 287 | 574 | 717 | 861 | 1434 |
| 4 | 0.92 | 161 | 323 | 646 | 807 | 969 | 1615 |
| 5 | 1.42 | 174 | 348 | 696 | 870 | 1044 | 1741 |
| Average | | 136 | 273 | 545 | 682 | 818 | 1363 |

Table 6. The translation of our specified k -cuts to ℓ -cut for our different tomographic bins, with the median redshift used to relate them (see Equation 1). The average over all five tomographic bins is given at the bottom of the table. We use the notation K_{\max} as this is not a true cut in k -space, but rather defined in k -space and applied as a cut in ℓ .

| Model Choice | ‘Test’ Mock | | ‘Truth’ Mock | | Bias | | |
|---|---------------------------|-------------------------|---------------------------|-------------------------|--------------|--|------------------------------|
| | S_8 | $S_8 - S_8^{\text{in}}$ | S_8 | $S_8 - S_8^{\text{in}}$ | ΔS_8 | $\sigma_{\text{Test}}/\sigma_{\text{Truth}}$ | $\sigma/\sigma_{\text{Fid}}$ |
| Fiducial | $0.802^{+0.005}_{-0.006}$ | 0.31σ | $0.799^{+0.005}_{-0.006}$ | -0.14σ | 0.45σ | 1.04 | 1.00 |
| Varying IA model: TATT | $0.801^{+0.006}_{-0.006}$ | 0.25σ | $0.799^{+0.005}_{-0.006}$ | -0.20σ | 0.45σ | 1.04 | 1.05 |
| Sensitivity to informative prior width: h_0 & n_s | $0.802^{+0.006}_{-0.006}$ | 0.38σ | $0.799^{+0.005}_{-0.006}$ | -0.12σ | 0.50σ | 1.03 | 1.03 |
| Varying sum of neutrino mass | $0.799^{+0.005}_{-0.005}$ | -0.28σ | $0.796^{+0.005}_{-0.006}$ | -0.76σ | 0.48σ | 0.98 | 0.95 |

Table 7. Y1 constraints on S_8 changing the intrinsic alignment model and varying the Y1 set of cosmological parameters and priors. The second row shows the impact on S_8 from using the TATT model for intrinsic alignments compared to the fiducial case using NLA- z , the third row shows the impact of using wider priors for h_0 and n_s and finally the last row shows the impact of marginalising over neutrino mass.

| Baryon Input | Analysis Model | ‘Test’ Mock | | ‘Truth’ Mock | | Bias | | |
|------------------------------|----------------|---------------------------|-------------------------|---------------------------|-------------------------|---------------|--|------------------------------|
| | | S_8 | $S_8 - S_8^{\text{in}}$ | S_8 | $S_8 - S_8^{\text{in}}$ | ΔS_8 | $\sigma_{\text{Test}}/\sigma_{\text{Truth}}$ | $\sigma/\sigma_{\text{Fid}}$ |
| Fiducial | HMCode2020 | $0.802^{+0.005}_{-0.006}$ | 0.31σ | $0.799^{+0.005}_{-0.006}$ | -0.14σ | 0.45σ | 1.04 | 1.00 |
| Strong Feedback | HMCode2020 | $0.795^{+0.006}_{-0.005}$ | -0.83σ | $0.794^{+0.006}_{-0.007}$ | -1.03σ | 0.20σ | 0.89 | 0.97 |
| Weak Feedback | HMCode2020 | $0.803^{+0.005}_{-0.006}$ | 0.59σ | $0.801^{+0.005}_{-0.006}$ | 0.23σ | 0.36σ | 1.04 | 0.93 |
| Fiducial | SP(k) | $0.801^{+0.005}_{-0.005}$ | 0.30σ | $0.802^{+0.005}_{-0.005}$ | 0.40σ | -0.11σ | 0.91 | 0.85 |
| Fiducial - all scales | SP(k) | $0.801^{+0.005}_{-0.005}$ | 0.27σ | $0.798^{+0.004}_{-0.004}$ | -0.41σ | 0.68σ | 1.19 | 0.84 |
| Strong Feedback | SP(k) | $0.794^{+0.005}_{-0.006}$ | -1.11σ | $0.795^{+0.005}_{-0.005}$ | -0.86σ | -0.25σ | 1.04 | 0.96 |
| Strong Feedback - all scales | SP(k) | $0.795^{+0.005}_{-0.004}$ | -1.14σ | $0.792^{+0.005}_{-0.005}$ | -1.86σ | 0.72σ | 0.93 | 0.79 |
| Weak Feedback | SP(k) | $0.803^{+0.005}_{-0.005}$ | 0.60σ | $0.804^{+0.005}_{-0.005}$ | 0.71σ | -0.11σ | 0.97 | 0.90 |

Table 8. Y1 Constraints on S_8 using different baryon feedback simulations in the mock and two different methods for modelling, HMCode2020 and SP(k). We additionally compare the constraints when using all angular scales up to $\ell_{\max} = 5000$ with cuts at $K_{\max} = 0.5$, our fiducial choice.